ELECTRONPROBE ANALYSES OF NICKEL DIFFUSION GRADIENTS IN IRON METEORITES AND THE COOLING HISTORY OF THE METEORITE PARENT-BODIES[1,2]

James M. Short*
Division of Geological Sciences
California Institute of Technology
Pasadena, California

and

Christian A. Andersen
Hasler Research Center
Applied Research Laboratories
Goleta, California

*Present Address: Space Sciences Division, Ames Research Center, National Aeronautics and Space Administration, Moffett Field, California

[1]Contribution No. 1295, Division of Geological Sciences, California Institute of Technology, Pasadena, California.

[2]Parts of this paper were presented at the April, 1964 meeting of the American Geophysical Union in Washington, D. C.

16345

Abstract. Compositional variations in nickel, iron, and cobalt in nine octahedrites were determined by electron microprobe X-ray analysis. The steep gradients in taenite extending up to 35-50 wt.% Ni and the shallow decreases (0.2-1 wt.% Ni) in kamacite near the interface of the kamacite and taenite phases were formed during the final stage of formation of the Widmanstatten structure as cooling prevented attainment of equilibrium by diffusion. A simplified theoretical model based on the Fe-Ni system was used to relate the extent of diffusion to cooling rates of the meteorite parent-bodies. These depend critically on assumptions concerning the nucleation temperatures of kamacite, pressure, phase equilibria, and cooling model. Metallurgical evidence implies that nucleation of kamacite may not have occured at the $\gamma / \alpha + \gamma$ boundry in the Fe-Ni system, but after undercooling of about 100°C at 1 atmosphere pressure. α_2 nuclei may have initiated diffusion growth of kamacite which ceased by 350°C. Differing nucleation temperatures account for meteorites of different structure, but identical nickel content, for a range of kamacite band-widths, and for coarse plessite. Fine plessite, of variable composition (10-28 wt.% Ni) developed after partial transformation of γ to α_2 below M_s. It seems most reasonable that the Widmanstatten structure formed at low pressures in 10^7-10^8 years at cooling rates of 2-12°C/10^6 years in the temperature interval 650-350°C. These are consistent with a chondritic parent-body (or bodies) with a metallic core and a radius of 100-200km.

AUTHOR

INTRODUCTION

The existence of high-nickel borders in the taenite phase of iron meteorites has been shown by previous electron microprobe X-ray analyses (Yavnel', et. al., 1958; Maringer, et. al., 1959; Feller-Kniepmeyer and Uhlig, 1961). These non-equilibrium nickel gradients are related to the formation of the Widmanstatten structure by phase precipitation and growth by solid state diffusion. Uhlig (1954) and Urey (1956) have tried to estimate the time for formation of the Widmanstatten pattern by using the simpliest diffusion parameters, as did Massalski and Park (1962) by use of the Fe-Ni phase diagram. The nickel diffusion gradients in the taenite phase of nine octahedrites, have been measured with an electron microprobe. A refined diffusion theory and cooling model was applied in order to determine the probable cooling rates and sizes of the meteorite parent-bodies.

EXPERIMENTAL METHODS

The meteorites were selected so as to provide a range of kamacite band-widths in all octahedrite classes and to represent all four Ge-Ga groups (Lovering, et.al., 1957). Octahedrites of different texture but similar nickel content were chosen—e.g., Bristol and Toluca—to test the hypothesis (Goldberg, et. al., 1951) that different band-widths might be due to different cooling rates.

Unweathered sections were cut with a carborundum wheel, polished with silicon carbide and diamond paste through 1 μ, then cleaned ultrasonically in benzene. No etching was done, in order to avoid surface redeposition (Feller-Kniepmeyer, 1961). The taenite bands and plessitic areas to be analyzed were selected by microscopic examination. Generally, the larger symmetrical bands of taenite or plessite between the primary kamacite bands defining the Widmanstatten structure were chosen. Particular care was used to avoid areas near intersecting band systems where diffusion had proceeded from two or more directions. Irregular areas or bands near inclusions were avoided. Figure 1 illustrates a typical band.

Analyses were made at the Scripps Institution of Oceanography, with a modified electron microprobe X-ray analyzer (Applied Research Laboratories, Glendale, California). The instrument was operated at 25 kv. with a probe diameter of less than 1 μ. Appropriate integration times and stop-counting gave precisions in measurements of $\pm$ 0.2%. The microprobe tracks were made perpendicular to the long surface

axis of the band near the center, as shown in Figure 1. The probe was stepped 1-9 μ between analyses, depending on the compositional gradient. Microscopic calibration confirmed the accuracy (0.2 μ) of the microprobe stepping mechanism.

Pure metals were used as standards for iron, nickel, and cobalt. A chemically analyzed schreibersite (15.5% P) in the meteorite Horse Creek was the phosphorus standard. All raw data were corrected for detector dead-time and background. Mass-absorption corrections were applied to nickel, iron, and cobalt; fluorescence corrections were applied to iron. Secondary fluorescence of cobalt by nickel K - β is negligible. The accuracy of the theoretical corrections was checked by comparison with chemically analyzed Fe-Ni alloys (International Nickel Company; furnished by J. Goldstein, Department of Metallurgy, Massachusetts Institute of Technology). The results are given in Table 1.

In the alloys the microprobe accuracy for nickel was better than ± 0.5%, and the accuracy for iron ± 1%. In meteorite areas where the composition changed across the diameter of the X-ray producing volume, the accuracy was less. In fine plessite, unresolvable by the microprobe, only average compositions could be determined, but in taenite, where the composition varied smoothly, an accurate concentration profile was easily obtained. In the areas of the meteorites where rhabdite or schreibersite was not present, the measured phosphorus content was very close to the detection limit of 200 ppm.

The orientation of the microprobe track relative to the $[\bar{1}10]_\alpha$ zone axis was determined by taking Laue photographs (molybdenum radiation) of the adjacent kamacite. Mehl and Derge (1937) have shown that during formation of the Widmanstatten structure the α-(110) planes of kamacite precipitate as plates parallel to the (110) planes of γ i.e., in the α-phase the direction of crystal growth by diffusion is the $[\bar{1}10]_\alpha$ zone axis. The angle between this direction of diffusion and the microprobe track was determined by indexing the Laue photographs and determining the corresponding angle between the $[\bar{1}10]_\alpha$ direction and the specimen normal.

RESULTS

Nickel profiles. Typical profiles of the nickel concentration across selected taenite or plessite bands are shown in Figures 2-11. The scales permit comparison between meteorites of the steepness of the concentration gradients, the distance ξ between the phase boundry and the nucleation point (see Appendix) the smoothness of the

gradient, and the central and bulk nickel concentration.

Most bands found in coarse and medium octahedrites (Figures 2-7) and narrow taenite bands found in fine octahedrites show the interior nickel content is higher than the bulk nickel content because nickel has diffused from the boundry to the center. Wide plessitic areas in fine octahedrites have the same average central nickel contents as the bulk concentration for the meteorite (Figures 8-10).

Symmetrical gradients across the entire taenite band were found only (e.g., Figures 2 and 6) when equal widths existed in the adjacent kamacite bands and the widths of the outer taenite bands were almost the same. When the above condition was not present profiles were usually observed, with the minimum nickel concentration in taenite lying off-center toward the narrower kamacite band (e.g., Figures 4,5, and 7). Assymmetric profiles were also observed when tracks were made at large angles relative to the [110] direction of kamacite or were near intersecting band systems such that diffusion had proceeded from more than one source. The central nickel content of taenite bands within one meteorite varies with the taenite band-widths, narrow bands showing proportionally higher nickel (e. g., Figures 4 and 5). Wider kamacite bands introduce more nickel into the bordering taenite, flattening the gradients at the border and raising the central taenite content (Figures 4 and 7). Figure 7 demonstrates the effect on the nickel-profiles of varying kamacite and taenite band-widths. The profiles are least affected near the α/γ boundry; in fact, they merge into a common gradient as they approach the boundry.

The kamacite was remarkably homogeneous except within 10-30 μ of the α/γ border. A slight structural dependence of mean nickel content of kamacite was observed: 6.6 wt. % for coarse octahedrites, 7.0 wt. % for medium octahedrites and 7.3 wt. % for fine octahedrites. At distances less than 10-30 μ from the boundry a continuous slight decrease in nickel was observed without exception as the boundry was approached, in agreement with observations by Yavnel' et.al. (1958) and Agrell, et.al., (1963). The decreases ranged from about 1% for coarse octahedrites (Figures 2-4) less for medium octahedrites (Figures 5-7) to only 0.2% - 0.3% for fine octahedrites (Figures 8-10). The extent of the decreases was correspondingly less. The decrease is real and not due to mass-absorption effects or sample preparation because: (a) it is independent of the direction of movement of the probe; (b) it is present whether or not the surface was finely or roughly polished; (c) it is present at all of the many interfaces analyzed; (d) taenite bands with steeper edge-gradients showed correspondingly shorter depression in kamacite.

Plessite. Microprobe analysis of plessite showed the same compositional variation that Perry (1944) observed. Coarse plessite, such as perthitic lamellas in coarse octahedrites, was resolvable with the microprobe into distinct taenite and kamacite regions; the fine plessite often occuring in fine octahedrites (Figures 8 and 9) was not resolvable; plessite of intermediate size (Figure 6) occurs frequently in medium octahedrites. Moving from the boundry toward the interior of taenite, the smooth nickel gradient starts showing fine structure of progressivily greater compositional variation at lower nickel concentrations (Figure 8 and 12), while the average plessite content follows the diffusion gradient until the interior is reached. Plessite in fine octahedrites had the same average composition as the bulk chemical content, provided enough microprobe analyses were made in plessite to give good statistics. Meteorites of fine structure have finer plessite than coarser octahedrites and have smaller amplitudes of nickel variation in plessite, as seen by comparison of Figures 6 and 8. The average nickel content of the kamacite in fine plessite approached about 6 wt. % and is lower than the nickel content of the kamacite in coarse plessite or the Widmanstatten structure.

The α/γ boundries in plessite, as seen in Figures 12 and 13, were not in straight octahedral orientation as was the case in the large Widmanstatten structure. Rather, warped boundries with preferred orientation were common. The existence of plessite does not always correlate simply with nickel content, even in one meteorite. Figure 3 shows a taenite band of which only one side has exsolved into plessite, while Figure 4 shows two taenite bands, of which the one with the higher nickel content has exsolved. The upper limit in nickel content for plessite occurence varies widely from approximately 14-28 wt. % nickel. There appears to be no lower limit for plessite formation; Bristol (Figure 10) has only 8.3 wt. % nickel, but has many areas of fine plessite.

Other elements. Iron was determined concurrently with nickel and invariably varied in an inverse manner, such that Fe + Ni $\cong$ 100%. Cobalt was measured in many bands and followed iron, with a α/γ distribution coefficient favoring kamacite, in agreement with observations by Nichiporuk (1958). Figure 11 shows a track across a taenite band in Canyon Diablo in which a pair of kamacite lamalle have apparently exsolved in the late stages of formation of the nickel gradients. The inverse correlation between nickel and cobalt is evident.

The phosphorus content of the metal-phase was at the detection limit (0.02%) in all meteorites except Canyon Diablo, in which infrequent rhabdite inclusions

occured and which had a central phosphorus content in kamacite 0.1%, but which decreased as taenite bands were approached.

Orientation studies. Table 2 lists the angle 90-θ between the track direction and the growth direction. A correction factor $\cos\Theta$ was applied to the measured profile distances (x') for diffusion calculations. In three cases (marked by *) subgrain-boundries had apparently caused imperfections in the crystal structure, the Laue photographs were diffuse, and no orientation could be determined. Such an effect is apparently independent of the perfection of the Widmanstatten structure (Derge and Kommel, 1937).

DISCUSSION

Phase transformations in the Fe-Ni system. The classic and generally accepted explanation for the formation of the Widmanstatten structure was offered by Derge and Kommel (1937) and Perry (1944). A homogeneous, solidified f.c.c. phase γ cooled slowly until the low-nickel b.c.c. phase (α or kamacite) nucleated and grew by solid state diffusion, absorbing iron and expelling excess nickel into the parent-phase taenite. The (110) crystallographic plane of the α-phase precipitated parallel to the (111) octahedral planes of the original γ-phase (Young, 1926; Mehl and Derge, 1937). Low-nickel hexahedrites had all of their γ-phase absorbed at lower temperatures as the meteorites bulk concentration passed back into the one phase region of α stability. The Fe-Ni phase diagram (Figure 14) approximates this sequence of events in general. The slope of the $\gamma/\alpha+\gamma$ boundry explains the general decreasing width of the Widmanstatten structure seen in Table 3 as the bulk nickel content increases. As the kamacite grew into the taenite, the interface concentrations at the moving boundry were dictated by the equilibrium phase compositions. The inhomogeneties seen in Figures 2-11 (gross in taenite; fine in kamacite) show that equilibrium was not maintained away from the kamacite-taenite interface. Rather, diffusion slowed down and was finally arrested at lower temperatures, leaving the gradients in nickel, iron and cobalt as evidence of a cooling process. These compositional gradients are quantitatively related to the cooling rate and times of formation of the Widmanstatten structure, which may be determined, provided the correct phase equilibria, nucleation and diffusion theory, and cooling model for the parent-body are assumed. The diffusion coefficient of nickel in γ, the total nickel content, the geometry and temperatures of nucleation of α, the cooling rates of the meteorite at these temperatures and

pressure as it effects these variables are the parameters which determine the size and form of nickel-profiles in the Widmanstatten structure.

The currently accepted Fe-Ni sub-solidus phase diagram (Figure 14) of Owen and Liu (1949) explains the formation of the Widmanstatten structure in general, although the nickel content of kamacite in octahedrites is higher than predicted. This may be because the $\alpha/\alpha+\gamma$ boundry lies to the right or because the boundry is shifted by the presence of a few tenths percent of phosphorus in solution (Ringwood and Kaufman, 1962). The 0.5% cobalt content will not shift the phase boundries significantly. Owen and Liu's (1949) $\gamma/\alpha+\gamma$ boundry and Goldstein's (1964) tentative $\alpha/\alpha+\gamma$ boundry are assumed to approximate the octahedrite systems. The decreases in the nickel content of kamacite near kamacite-taenite boundries are most easily explained if the $\alpha/\alpha+\gamma$ boundry in the meteoritic phase system moves to less nickel content at lower temperature, (400-350°C) where boundry movement ceases and kamacite cannot homogenize.

Vogel (1925, 1951, 1937) has hypothesized that the Widmanstatten structure formed during a high temperature exsolution of α, as dictated by the Fe-Ni-P system. However, this seems unlikely, since the phosphorus content of octahedrites is too low (0-0.5% P); also no correlation of structure with phosphorus content exists. Even more significantly, it is calculated by Equations 1 and 2 that even as low as 1100°C, homogeneous γ-phase of 5 cm can be formed.

The kinetics of sub-solidus phase transformation in the Fe-Ni system have been misunderstood frequently in the past. It is of critical importance in interpretating the Widmanstatten structure to define the nucleation temperatures of kamacite. This is probably not at the temperature at which the bulk composition crosses the $\gamma/\alpha+\gamma$ boundry, but at some lower temperature. Cooling experiments on artificial alloys by Jones and Pumphrey (1949), Allen and Earley (1950) and Kaufman and Cohen (1956), as well as earlier heating experiments of Hanson and Hanson (1920) and Owen and Sully (1939) have shown that, upon cooling, γ-phase undercools below the $\gamma/\alpha+\gamma$ phase boundry. At the temperature M_s the f.c.c. γ-structure starts to change by a diffusionless transformation to α_2, a strained b.c.c. structure of the same composition. Annealing or very slow cooling permits α_2 to decompose into $\alpha+\gamma$, in accordance with the phase diagram.

Kaufman and Cohen (1958, 1956) have reviewed the thermodynamics of the transformation and showed that at T_o $\Delta F(\gamma \rightarrow \alpha_2) = 0$. Further undercooling in Fe-Ni alloys from T_o to M_s is required because of interfacial and strain energy contributions to the free energy. The transformation is not complete until a still lower temperature

M_f is reached. The M_s and T_o temperatures shown in Figure 14 are not accurately known and may vary. M_s may be raised or lowered by impurities; cobalt increases M_s slightly (Yeo, 1963). Stress increases M_s by 10-15°C/kb., and pressure lowers M_s by 6°C/kb. (Patel and Cohen, 1953). Likewise, pressure lowers the equilibrium phase boundries (Ringwood and Kaufman, 1962), and phosphorus raises them (Vogel, 1951). However, for reasons given by Ringwood and Kaufman (1962) and the diffusion calculations below, minor components in meteorites do not seem to have affected the phase boundries significantly. Thus the $\gamma/\gamma + \alpha$ boundry and M_s in the Fe-Ni system may be taken as giving approximate upper and lower limits on the temperature at which b.c.c. formed in iron meteorites.

If one extrapolates the studies on artificial alloys to geologic time intervals (an assumption that does not contradict present experimental evidence), undercooling of γ as far as M_s is possible. Given sufficient time at temperatures between T_o and M_s, α_2 nuclei might exceed the activation barrier for formation and quickly grow as a very thin (μ-size) plate parallel to the $(111)_\gamma$ plane, stopping laterally only when a grain boundry or another α_2 was encountered. This b.c.c. phase would then be the nucleus for decomposition into the equilibrium $\alpha + \gamma$. The assumption of different degrees of undercooling is supported by the data in Figures 2-11, since kamacite bands of widely varying width are seen in the same meteorite; these have expelled differing amounts of nickel into taenite. The assymetric taenite bands with different nickel-distance profiles are also explained by different nucleation temperatures for the adjacent kamacite bands. Local compositional differences are probably too small to account for these effects, since the average microprobe analysis of fine plessite (e.g., Altonah) is the same as the bulk composition. Meteorites of different mean kamacite band-width, but identical nickel content (see Massalski, 1962) could also have had different average nucleation temperatures, rather than different cooling rates, as Goldberg, et.al. (1951) hypothesized.

Since the gross Widmanstatten pattern suggests nucleation and growth of α in γ rather than growth of γ in α_2, the assumption most consistent with studies on artificial alloys is that nucleation occured some place between T_o and M_s, the temperature at which α_2 becomes thermodynamically stable. Once formed, the α_2 nuclei would permit normal $\alpha + \gamma$ -phase segregation. Bowles and Barrett (1952) have suggested that the martensitic mechanism may be operative in the early stages of nucleation and growth from solid solution. The mechanism proposed here differs somewhat from Owen's (1940) hypothesis that the Widmanstatten structure formed by decomposition of α_2 below M_s in that α_2 nucleates the growth of α in γ. Random

nucleation at different temperatures between T_o and M_s would then permit kamacite bands of different widths to develop in the same meteorites or in meteorites with the same bulk composition but different structure. Nucleation of Widmanstatten growth at M_s seems unlikely, since all γ-phase (< 30% Ni) would have instantaneously transformed to α_2, requiring γ to grow in α_2.

An explanation for the genesis of the Widmanstatten structure is incomplete without accounting for the origin and nature of plessite. The coarse plessite consisting of narrow lamellas of kamacite and taenite is simply understood in terms of lower temperature nucleation of α from γ (Derge and Kommel, 1937). This occurs naturally in bands of taenite with relatively low nickel content (e.g., Figure 6). Likewise the octahedrally oriented needles of kamacite which are often observed in the center of larger taenite bands are also understood as having formed like the large Widmanstatten pattern, but at lower temperatures with slower diffusion rates because of the higher interior nickel content of the taenite. Furthermore, the presence of kamacite spindles with octahedral orientation in nickel-rich ataxites (Perry, 1944) shows that the mechanism of Widmanstatten-pattern formation extends into the plessitic nickel-rich ataxites. This implies that Uhlig's (1954) cut-off of the Widmanstatten structure at 13% nickel (17%, Table 3) is meaningful only as a large-scale textural description, and the same mechanism operates at higher nickel contents and correspondingly lower temperatures, but on a necessarily smaller scale. The narrow kamacite plates does not extend throughout nickel-rich ataxites because the nucleation was localized.

The formation of fine plessite seems to require a different mechanism than merely lower nucleation temperatures due to higher nickel content. The phase orientations seen in the fine plessite of Figures 12 and 13 lack sharp parallel octahedral boundries. The random micro-taenite particles shown in Figures 8 and 9 suggest the possibility that they grew from kamacite, rather than the reverse. The dimensions of plessitic phases are discontinuous with the general dimensions of the Widmanstatten structure: this would not be expected in fine octahedrites (Figures 8-10) if a range of nucleation temperatures were possible. It is suggested that Owen's (1940) hypothesis of the origin of plessite is applicable to the formation of fine plessite. Undercooled γ-phase eventually reached the M_s temperature (Figure 14) and started to be transformed to b.c.c., α_2-phase, which then decomposed into $\alpha + \gamma$, provided the temperatures were high enough to permit diffusion. The temperatures would be too low when transformation took place in the high nickel borders of taenite. Imperfect phase orientations would be expected. The mechanism is in agreement with laboratory

studies of the kinetics of Fe-Ni alloys and with the widespread occurence of fine plessite in meteorites. It also explains the occurence of nickel-rich ataxites of low nickel content. The general textural uniformity of fine plessite within fine octahedrites also suggests widespread nucleation at a particular temperature dictated by C_b.

Diffusion theory. The solutions of the diffusion equations to represent the concentration gradients shown in Figures 2-10 is a difficult problem, involving non-isothermal phase growth with changing boundry conditions. It has not been attempted to derive an exact solution for the concentration-distance profiles, but rather, to derive appropriate diffusion parameters which may be related to thecooling rates and times of formation of the Widmanstatten pattern and subsequently to parent-body sizes of the meteorites upon assumption of an appropriate cooling model. The kamacite bandwidths and the amount of nickel transferred across the α/γ interface during phase growth are critically dependent upon the temperature of nucleation, the diffusion coefficient and the cooling rate of the meteorite within the temperature range of boundry movement. Because nickel in γ is the slowest diffusing species, (Hirano, et. al., 1961) D (nickel, γ) controls the rate of α/γ boundry movement. Recent accurate interdiffusion measurements of D (nickel, γ) by Goldstein et.al. (1964), which may be extrapolated to 500°C with only ± 50% error, were used to calculate tne cooling rate r during Widmanstatten pattern formation by use of the expression (Armstrong, 1958)

$$r \cong \frac{D_n R T_n^2}{F E} \qquad (1)$$

where D_n is D at the nucleation temperature T_n, r is the linear cooling rate, E is the activation energy for diffusion, and F is a diffusion parameter (see Appendix) calculated from

$$\xi = 2\bar{\gamma}\sqrt{F} \qquad (2)$$

ξ is the amount of kamacite boundry movement since α-nucleation, and γ is evaluated from the boundry conditions.

The possible cooling rates for each meteorite were calculated at four temperatures, including M_s, T_o, and the temperature at which the bulk concentration C_b intersects the $\gamma/\alpha+\gamma$ boundry. These are plotted against $1/T_n$ in Figure 15.

The general slope is given by the activation energy for D (nickel, γ); minor variations are due to differing C_b and γ. The meteorites are listed in order of decreasing coarseness of structure, and different ξ and F values account for the spread of the lines. The average cooling rate for nucleation at T_o for seven octahedrites (excluding Bristol and Altonah) is $0.04^{\circ}C/10^4$ yrs. Bristol and Altonah either cooled somewhat faster or undercooled closer to M_s. The identity of their cooling rates, diffusion gradients (compare Figures 9 and 10), and chemical composition (Goldberg, et. al., 1951; Nichiporuk and Brown, 1964) suggest that they are genetically related.

The particular band or bands studied in each meteorite have unique nucleation temperatures and band-widths, which are not necessarily representative of the mean (Table 3) band in the meteorite, nor in its class (Og, Om, or Of). The mean nickel contents and kamacite band-widths of octahedrite classes (Table 3) were obtained by calculating averages of the "superior" modern nickel analyses by Goldberg, et. al., (1951), Lovering et al (57) and others and of kamacite band-width measurements of Lovering (1956) and Goldberg, et. al., (1951). ξ is given by one half the mean band-width corrected by a factor of 0.8 to compensate for band width measurements made on meteorite sections which were not parallel to the original direction of diffusion. The corresponding cooling rates for coarse, medium and fine octahedrites are also plotted in Figure 15.

At T_o they are almost the same, averaging $0.12^{\circ}C/10^4$ yrs. Assuming that the degree of undercooling did not vary widely for different meteorites, it seems likely that the cooling rates during Widmanstatten-pattern formation are very nearly the same for all octahedrites. This condition implies that octahedrites were once at the same depth in a single parent-body or had the same cooling environment at 600°C in several bodies.

Octahedrite parent-bodies. The nature of the meteorite parent-bodies has been discussed by many workers (Anders, 1961, 1964; Fish, et. al., 1960; Goles, et. al., 1960; Lovering, 1957 a, b, 1962; Mason, 1960, 1962; Ringwood, 1961; Urey, 1958, 1959, etc.). One of the simplest cooling models assumes that iron meteorites cooled from the melt in the center of a differentiated planet with a chondritic mantle. The relation (see Appendix) between the central cooling rate and the radius of the body is shown in Figure 16.

Long-lived radioactivity (K^{40}, U^{235}, U^{238}, Th^{232}) decreases cooling rates somewhat in bodies larger than 200 km. Figure 17 shows the corresponding parent-body radii for different nucleation temperatures; the comments made on Figure 15 apply also to Figure 17. For nucleation at T_o, the average radius for seven octahedrites, is 160 km., and Og, Om, and Of octahedrites could have cooled in a body of 100 km radius. For nucleation between T_o and M_s, a 170 km body would account for all twelve cases considered. For example, an average medium octahedrite, cooling at the core of a chondritic body of this size at a rate of $2.5^{\circ}C/10^6$ yrs., would undercool 130°C to 590°C before nucleating, and formation of the Widmanstatten structure would be complete in less than 10^8 yrs. The chondritic body would have required about $3 \cdot 10^8$ yrs. to cool from 1800°K to 350°C.

Pressure is a parameter which must be considered, because of its effect on phase boundries and diffusion rates. High pressures over 10 kb. significantly depress the $\gamma/\alpha+\gamma$ boundry in the Fe-Ni system (Ringwood and Kaufman, 1961). Uhlig (1954) used this effect to explain the rarity of the Widmanstatten structure >13% nickel. However, the existence of undercooling of about 100°C and the occurence of micro-Widmanstatten patterns in nickel-rich ataxites (Perry, 1944) make this assumption of high static pressure unnecessary. It can be shown by use of Equation (9) (Appendix) that planetary-bodies greater than about 400 km radius (with central pressures of 4 kb.) cannot even have cooled from 1800°K to 350°C at the center in $4.5 \cdot 10^9$ yrs. This was also pointed out by Allan and Jacobs (1956) and Urey (1956). Furthermore, Goldstein (1964) has shown that static pressure strongly decreases the diffusion coefficient of nickel in γ-phase, such that it appears impossible to form coarse Widmanstatten structures under high pressure, even with no undercooling.

The possibility can also be considered that the cooling rates calculated here could be due to octahedrites cooling in pockets near the surface of larger bodies, as envisioned by Henderson and Perry (1958) and Urey (1959). Even so, low pressures are required. Anders and Goles (1961) state other arguments against such a model.

Perhaps more complex combinations of pressure, phase equilibria, and cooling model might be devised as our understanding of iron-pallasite-chondrite relationships grows. For example, Carter and Kennedy (1964) suggest that parent-bodies capable of producing diamond might have disrupted at temperatures above 800°C, then cooled more rapidly as the Widmanstatten structure developed. However, this hypothesis seems inconsistent with the strong general correlation of nickel-content with kamacite bandwidths, and the similar cooling rates calculated for the meteorites studied.

Acknowledgements. We wish to thank Professor G. Arrhenius of the Scripps Institution of Oceanography for providing electron microprobe facilities and Professor P. Duwez of the California Institute of Technology for the use of Laue X-ray equipment. Professor H. Brown of the California Institute of Technology gave aid and encouragement. J. I. Goldstein graciously provided diffusion coefficients in the Fe-Ni system in advance of publication. Helpful discussions were held with J. I. Goldstein, H. Brown, W. Nichiporuk, H. H. Uhlig, J. A. Wood, F. S. Buffington, and K. Fredricksson.

This research was supported by NASA grants No. NsG 56-60 and NsG 317-63.

APPENDIX

Diffusion theory. Solutions of the diffusion equation for a constant diffusion coefficient D may be used for time-dependent diffusion coefficients by employing the parameter F (Crank, 1956) defined by

$$F = \int_0^t D(t)\, dt \qquad (1)$$

For the case of a linear cooling rate r, Armstrong (1958) derived an approximate expression for F

$$F \cong \frac{D_n R T_n^2}{rE} \qquad (2)$$

D_n is D at the nucleation temperature T_n, r is the cooling rate, and E is the activation energy for diffusion. By combining Equation (2) with expressions for T (t) and D (t), one can derive a relation for the time t_{n-f} for formation of the Widmanstatten structure between T_n and T_f, a temperature at which lower diffusion rates cause negligible boundry movement

$$t_{n-f} = \frac{F\ T_f}{D_n\ T_n} \ln \frac{D_n}{D_f} = \frac{F\ E(T_n - T_f)}{D_n\ R\ T_n^2} \qquad (3)$$

Jost (1952) has given analytical solutions to the diffusion equation for isothermal moving-boundry problems in two phases. For the purposes of approximation, we will assume by analogy with Jost, that the following relation is sufficiently correct for linear cooling rates over fairly narrow temperatures ranges:

$$\xi = 2\gamma\sqrt{F} \tag{4}$$

ξ is the amount of boundry movement and γ is a dimensionless parameter dependent upon the boundry conditions. Since the observed kamacite is almost homogeneous, ξ may be determined by

$$\begin{aligned} \xi'(C_b - C_a) &= A \\ \xi &= \xi' \cos\theta \end{aligned} \tag{5}$$

where A is the total amount of nickel expelled into the γ-phase. A is determined by integration of the nickel-concentration-distance profile in taenite above C_b to the minimum in the profile. If the boundry conditions are constant, γ may be evaluated (Jost, 1952) from the expression

$$\frac{Q}{Q+1} = \sqrt{\pi}\,\gamma e^{\gamma^2}\,\operatorname{erfc}\gamma \tag{6}$$

where $Q = (C_{II} - C_b)/(C_b - C_I)$. C_{II} and C_I are the respective nickel concentrations at the interface between the γ and α-phases. Figure 18 shows that Q can vary greatly between T_n and T_f, but γ varies much less. Because of the exponential decrease of D with temperature, most of the phase growth and material transport across the interface occurs at and just below T_n, with relatively small changes in boundry conditions; Therefore, Equation (4) may be assumed to hold approximately, using a mean γ, $\bar{\gamma}$. Assuming that one half of the total material transport takes place by the time that D has decreased to $D_n/4$ (at $T_n - 30^\circ C$), a mean $\bar{Q}$ (and $\bar{\gamma}$ by Figure 18) is given by

$$\bar{Q} = Q_n + \Delta Q \tag{7}$$

$$\frac{\Delta Q}{Q_f - Q_n} = \frac{T_n - 30}{T_n - T_f} \tag{8}$$

since Q and T may both be assumed to vary linearly with time. With ξ and $\bar{\gamma}$ determined F may be calculated by Equation (4), and r determined by Equation (2) for assumed temperatures of nucleation.

The nickel-profile in taenite approaches the α/γ asymptotically, so the equilibrium concentration can not be correlated with the kamacite composition. For practical purposes and for the resolution of the microprobe, Equations (2) and (4) were used to fix T_f at 350°C, corresponding to a C_{II} of 48.5 atom % nickel as plotted in Figures 2-11.

Cooling model. The formula (Allan and Jacobs, 1956) for the central temperature T_c of a sphere of radius R with thermal diffusivity α and surface temperature T_s cooling from an initial temperature T_i is given by

$$\frac{T_c - T_s}{T_i - T_s} = 2 \sum_{m=1}^{\infty} (-1)^{m+1} e^{-m^2 \pi^2 \alpha t / R^2} \qquad (9)$$

$\pi^2 \alpha t/R^2$ may be extracted with tables of Ingersoll and Zobel (1948), for T_n and T_f and R calculated. T_i was taken as 1800°K, the minimum temperature at which liquid metal and silicate could have differentiated. α was assumed to be $7 \cdot 10^{-2} cm^2/sec.$, the approximate thermal conductivity for chondrites, as calculated from data compiled by Wood (1963). $T_s = 100°K$, the approximate temperature in the asteroid belt.

REFERENCES

Agrell, S. O., J. V. P. Long, and R. E. Ogilvie, Nickel content of kamacite near the interface with taenite in iron meteorites, Nature, 4882, 749-750, 1963.

Allan, D. W. and J. A. Jacobs, The melting of asteroids and the origin of meteorites, Geochim. et Cosmochim. Acta, 9, 256-272, 1956.

Allen, N. P. and C. C. Earley, The transformations $\alpha \rightarrow \gamma$ and $\gamma \rightarrow \alpha$ in iron-rich binary iron-nickel alloys, J. Iron Steel Inst. (London), 166, 281-288, 1950.

Anders, E., Origin, age, and composition of meteorites, Space Science Reviews, in press, 1964.

Anders, E., and G. G. Goles, Theories on the origin of meteorites, J. Chem. Ed., 38, 58-66, 1961.

Armstrong, H. L., On solid-state diffusion with a linearly varying temperature, Trans. AIME , 212, 450-451, 1958.

Bowles, J. S. and C. S. Barrett, Crystallography of transformations, Progress in Metal Physics, 3, 1-41, 1952.

Carter, N. L. and G. C. Kennedy, Origin of diamonds in the Canyon Diablo and Novo Urei meteorites, J. Geophys. Res., 69 (12), 2403-2421, 1964.

Crank, J., The Mathematics of Diffusion, p. 146 , Clarenden Press, Oxford, 1956.

Derge, G. and A. R. Kommel, The structures of meteoric irons, Am. J. Sci., 34, 203-214, 1937.

Feller-Kniepmeyer, M. and H. H. Uhlig, Nickel analyses of metallic meteorites by the electronprobe microanalyzer, Geochim. et Cosmochim. Acta, 21, 257-265, 1961.

Fish, R. A., G. G. Goles, and E. Anders, The record in the meteorites, III. On the development of meteorites in asteroidal bodies, Astrophys. J., 132, 243-258, 1960.

Goldberg, E., A. Uchiyama, and H. Brown, The distribution of nickel, cobalt, gallium, palladium and gold in iron meteorites, Geochim. et Cosmochim. Acta, 2, 1-25, 1951.

Goldstein, J. I., The growth of the Widmanstatten pattern in metallic meteorites, Ph.D. thesis, Massachusetts Institute of Technology, 1964. Submitted to Geochim. et Cosmochim. Acta, 1964.

Goldstein, J. I., R. E. Hannemand, and R. E. Ogilvie, Diffusion in the iron-nickel system at 1 atmosphere and at 40 kbar., submitted to Trans. AIME, 1964.

Goles, G. G., R. A. Fish, and E. Anders, The record in meteorites - I The former environment of stone meteorites as deduced from K^{40}-Ar^{40} ages, Geochim. et Cosmochim. Acta, 19, 177-195, 1960.

Hanson, D. and H. E. Hanson, The constitution of Ni-Fe alloys, J. Iron Steel Inst., 102, 39-60, 1920.

Henderson, E. P., El Burro, Coahuila, Mexico, meteorite, Am. Min., 26, 655-656, 1941.

Henderson, E. P. and S. H. Perry, A discussion of the densities of iron meteorites, Geochim. et Cosmochim. Acta, 6, 221-240, 1954.

Henderson, E. P. and S. H. Perry, Studies of seven siderites, Proc. U. S. Natl. Museum, 107, 339-403, 1958.

Hirano, K. M. Cohen, and B. L. Averbach, Diffusion of nickel into iron, Acta Met., 9, 440-445, 1961.

Ingersoll, L. R., O. J. Zobel, and A. C. Ingersoll, Heat Conduction, With Engineering and Geological Applications, Appendix H, McGraw-Hill, New York, 1948.

Jones, F. W. and W. I. Pumphrey, Free energy and metastable states in the iron-nickel and iron-manganese systems, J. Iron Steel Inst. (London), 163, 121-131, 1949.

Jost, W., Diffusion in Solids, Liquids, Gases, pp. 68-75, Academic Press, New York, 1952.

Kaufman, L. and M. Cohen, The martensitic transformation in the iron-nickel system, Trans. AIME, 206, 1393-1401, 1956.

Kaufman, L. and M. Cohen, Thermodynamics and kinetics of martensitic transformations, Progress in Metal Physics, 7, 165-246, 1958.

Lovering, J. F., Structural and compositional studies on selected phases of iron and stony-iron meteorites, Ph. D. thesis, California Institute of Technology, 1956.

Lovering, J. F., Differentiation in the iron-nickel core of a parent meteorite body, Geochim. et Cosmochim. Acta, 12, 238-252, 1957a.

Lovering, J. F., Pressures and temperatures within a typical parent meteorite body, Geochim. et Cosmochim. Acta, 12, 253-261, 1957b.

Lovering, J. F., The evolution of the meteorites--evidence for the co-existence of chondritie, achondritic, and iron meteorites in a typical parent meteorite body, in Researches on Meteorites, edited by Carleton B. Moore, pp. 179-198, John Wiley and Sons, New York, 1962.

Lovering, J. F. and C. A. Andersen, to be submitted to Science, 1964.

Lovering, J. F., W. Nichiporuk, A. Chodos, and H. Brown, The distribution of gallium, geranium, cobalt, chromium, and copper in iron and stony-iron meteorites in relation to nickel content and structure, Geochim. et Cosmochim. Acta, 2, 263-278, 1957.

Maringer, R. E., N. A. Richard, and A. E. Austin, Microbeam analysis of Widmänstatten structure in meteoric iron, Trans. AIME, 215, 56-58, 1959.

Mason, B., The origin of meteorites, J. Geophys. Res. 65, 2965-2970, 1960.

Mason, B., Meteorites, pp. 192-200, John Wiley and Sons, New York, 1962.

Massalski, T. B., Some metallurgical aspects of the study of meteorites, in Researches on Meteorites, edited by Carleton B. Moore, pp. 107-122, John Wiley and Sons, New York, 1962.

Massalski, T. B. and F. R. Park, A quantitative metallographic study of five octahedrite meteorites, J. Geophys. Res., 67, 2925-2934, 1962.

Meen, V. B., The composition of the Maria Elena meteorite, Am. J. Sci., 239, 412, 1941.

Mehl, R. F. and G. Derge, Studies upon the Widmanstatten structure, VIII the $\gamma - \alpha$ transformation in Fe-Ni alloys, Trans. AIME, 125, 482-500, 1937.

Nichiporuk, W., Variations in the content of nickel, gallium, germanium, cobalt, copper and chromium in the kamacite and taenite phases of iron meteorites, Geochim. et Cosmochim. Acta, 13, 233-247, 1958.

Nichiporuk, W. and H. Brown, The distribution of platinum and palladium metals in iron meteorites and in the metal phase of ordinary chondrites, submitted to J. Geophys. Res., July, 1964.

Owen, E. A., The structure of meteoritic iron, Phil. Mag., 29, 553-567, 1940.

Owen, E. A. and Y. H. Liu, Further X-ray study of the equilibrium diagram of the iron-nickel system, J. Iron Steel Inst. (London), 163, 132-137, 1949.

Owen, E. A. and A. H. Sully, Equilibrium diagram of iron-nickel alloys, Phil. Mag., 27, 614-636, 1939.

Patel, J. R. and M. Cohen, Criterion for the action of applied stress in the martensitic transformation, Acta Met., 1, 531-538, 1953.

Perry, S. H., The metallography of meteoric iron, U. S. Nat. Museum Bull., No. 184, 206 pp., 1944.

Prior, G. T., Catalogue of Meteorites, second edition, revised by M. H. Hey, 432 pp., British Museum, London, 1953.

Ringwood, A. E., Chemical and genetic relationships among meteorites, Geochim. et Cosmochim. Acta, 24, 159-197, 1961.

Ringwood, A. E. and L. Kaufman, The influence of high pressure on transformation equilibria in iron meteorites, Geochim. et Cosmochim. Acta, 26, 999-1009, 1962.

Uhlig, H., Contribution of metallurgy to the origin of meteorites. Part I-Structure of metallic meteorites, their composition and the effect of pressure, Geochim. et Cosmochim. Acta, 6, 282-301, 1954.

Urey, H. C., Diamonds, meteorites, and the origin of the solar system, Astrophys. J., 124, 623-637, 1956.

Urey, H. C., The early history of the solar system as indicated by the meteorites, Proc. Chem. Soc. (London), 57-78, 1958.

Urey, H. C., Primary and secondary objects, J. Geophys. Res., 64, 1721-1737, 1959.

Vogel, R., Über die Struktur der Eisen-Nickel-Meteoriten, Z. anorg. u. allgem. Chemie. 142, 193-228, 1925.

Vogel, R., Das System Eisen-Nickel-Phosphor und das meteorische Eisen, Handbuch der Metallphysik, II, 578-587, 1937.

Vogel, R., Die Gefugeformen des Meteoreisens und ihre Erklarung auf Grund des Zustandsdiagrammes des Systems Eisen-Nickel-Phosphor, Neues Jahrb. Mineral. Abhandl., 83, 23-52, 1951.

Wood, J A., Physics and chemistry of meteorites, Chap. 12 in The Moon, Meteorites, and Comets, (Vol. IV of The Solar System), edited by B. Middlehurst and G. Kuiper, U. of Chicago Press, Chicago, 1963.

Yavnel', A. A., I. B. Borovski, N. P. Ilin, and I. D. Marchukova, A study of the composition of the phases of meteoritic iron by means of a local X-ray spectral analysis, Doklady Akad. Nauk S S S R, 123, 256-258, 1958.

Yeo, R. B. G., The effects of some alloying elements on the transformation of Fe-22.5% Ni alloys, Trans. AIME, 227 (4), 884-890, 1963.

Young, J., The crystal structure of meteoric iron as determined by X-rays, Proc. Roy. Soc. (London), 112, 630-641, 1926.

TABLE I. Analysis of Standard Fe-Ni Alloys

Weight % Ni		Weight % Fe	
Chemical	Probe	Chemical (100-Ni)	Probe
5.15	5.30	94.85	95.66
10.26	9.82	89.74	90.83
15.10	15.13	84.90	85.32
19.25	18.99	80.75	80.24
25.17	25.45	74.83	75.79
36.46	35.62	63.54	65.52
50.28	49.07	49.72	51.31

TABLE 2. Meteorites Studied

Meteorite	Mean Kamacite band-width mm.	Ref. #	Assumed Ni content wt. %	Ref. #	Ge-Ga group (Lovering, et al 1957)	Angle between (110) and specimen normal	Average kamacite content wt. % Ni
Arispe	3 - 4	1	6.8	1	II	80°	6.7
Youndegin	2	2	6.9	4	I	67°	6.7
Canyon Diablo	2.2	1	7.2	1	I	74°	6.8
Toluca (Xiquipilco)	0.90	2	8.3	1	II	62°	6.8
Spearman	1.25	1	8.4	1	III	*	7.1
Sacramento Mts.	-	3	8.1	1	III	*	6.9
Duchesne	0.25	2	9.6	5	IV	83°	7.3
Bristol	0.24	1	8.3	5, 6	IV	49°	7.4
Altonah	0.36	1	8.7	6	IV	*	7.34 ± .07

References:

(1) Goldberg, et.al. (1951)

(2) Lovering (1956)

(3) Goldberg, et. al. (1951)

(4) Lovering, et. al. (1957)

(5) Nichiporuk (1958)

(6) Microprobe analysis of plessite

*Laue photograph diffuse

TABLE 3. Textural Classification of Iron Meteorites

Class	Mean Ni Composition	Mean band-width mm	Range of Ni - wt. %	Meteorites nearest limits	Ni content wt. %	Reference #
hexahedrites (H)	5.65(15)*	-----	5.5-6.0	Chilean Hex (7)	(5.60)	1
				Sandia Mts.	(5.94)	2
coarse octahedrites	6.8 (20)	2.5	6.0-7.3	El Burro (trans.)	(6.02)	3
				Odessa	(7.24)	2
very coarse Ogg	6.7 (9)	3	6.0-7.0	Youndegin	(6.92)	4
course Og	6.9 (11)	2.2	6.4-7.3	Mount Dooling	(6.41)	4
medium octahedrites Om	8.3 (28)	1.0	7.3-10.0	Albuquerque	(7.39)	2
				Roper River	(9.91)	4
fine octahedrites	10 (16)	0.3	7.6-17	Maria Elena	(7.71, 7.63)	2,5
				Tazewell	(17.1)	2
fine Of	9.1 (12)	0.32	7.6-13	Edmonton	(12.66)	2
very fine Off	13 (14)	0.16	10 —17	Ballinoa	(10.06)	4
Ni-rich ataxites	-----	-----	9 —68	Perryville	(9.63)	2
				Oktibbeha Ct.	(62)	6
plessitic ataxites	-----	$\propto$ spindles	9 —30	Limestone Creek	(30)	6
taenitic ataxites	-----	$\leq$ 0.2	30 —68	Santa Catharina	(32)	7

References: (1) Henderson (1954); (2) Goldberg, et.al., (1951); (3) Henderson (1941); (4) Lovering, et.al., (1957); (5) Meen (1941); (6) Prior (1953); (7) Lovering and Anderson (1964)

*( ) Indicates number averaged; analyses from references listed

LEGENDS FOR ILLUSTRATIONS

Figure 1. Photomicrograph of plessite band in Duchesne. Arrow shows typical position and direction of microprobe tracks. Scale bar 100 μ.

Figure 2. Nickel concentration-distance profile across taenite band in Youndegin (Og). ——— shows bulk nickel content. ξ' calculated amount of boundry movement, and x' are measured on section surface.

Figure 3. Profile of nickel content across taenite band in Arispe (Og). Peak nickel content in taenite established by diffusion calculation and numerous microprobe analyses.

Figure 4. Two profiles of nickel content in taenite and kamacite bands in Canyon Diablo (Og). Narrow band shows plessite.

Figure 5. Profiles of nickel across narrow and wide bands in Toluca (Om).

Figure 6. Taenite band with central fine structure in Sacramento Mts. (Om).

Figure 7. Effects of varying band-widths on taenite profiles in Spearman (Om).

Figure 8. Profile near edge of fine plessite area in Duchesne (Of). Horizontal line shows average plessite concentration.

Figure 9. Profile across fine plessite band in Altonah (Of), showing average central plessite concentration.

Figure 10. Profile across half of plessite area in Bristol (Of).

Figure 11. Variations of nickel and cobalt across a taenite band in Canyon Diablo having two coarse plessite lamellas.

Figure 12. Electron back-scatter picture at border of taenite and plessite (top) in Duchesne. Lighter areas are nickel-rich. Scale bar 5μ.

Figure 13. Electron back-scatter picture of nickel in interior of fine plessite in Duchesne. Lighter areas are taenite. Scale bar 5 μ.

Figure 14. Portion of Fe-Ni sub-solidus phase diagram at 1 atm. pressure, α / α + γ

boundry is uncertain. M_s and T_o refer to $\gamma \rightarrow \alpha_2$ transformation.

Figure 15. Calculated cooling rate of meteorite during formation of Widmanstatten structure for different assumed kamacite nucleation temperatures (T_n) given by Figure 14.

Figure 16. 1 - Cooling rate at center of sphere with initial temperature 1800°K, surface temperature 100°K, and α = 0.007 cm.^{2}/sec.

2 - Effect of long-lived radioactivity.

Figure 17. Calculated parent-body radius of meteorite at center during formation of Widmanstatten structure for different assumed kamacite nucleation temperatures (T_n) given by Figure 14.

Figure 18. Boundry-condition diffusion parameter γ as a function of bulk content C_b and boundry concentrations C_γ and C_α in γ and α phases.

Figure I

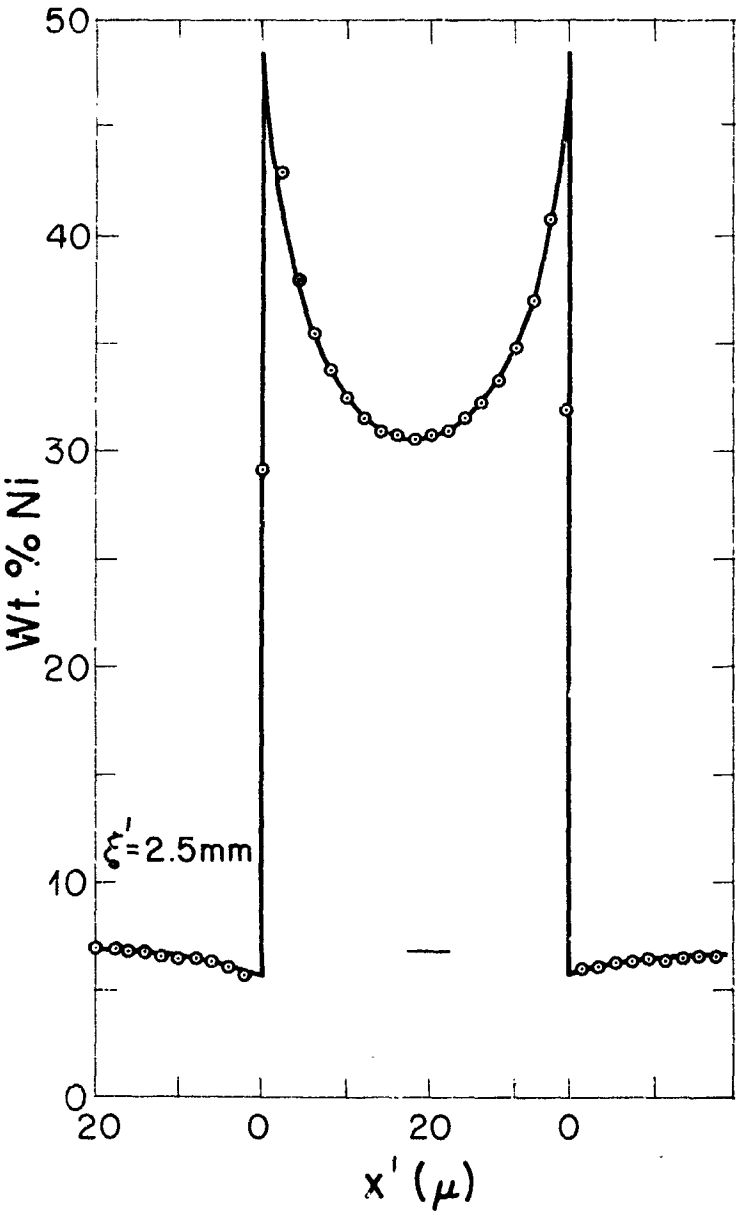

Figure 2

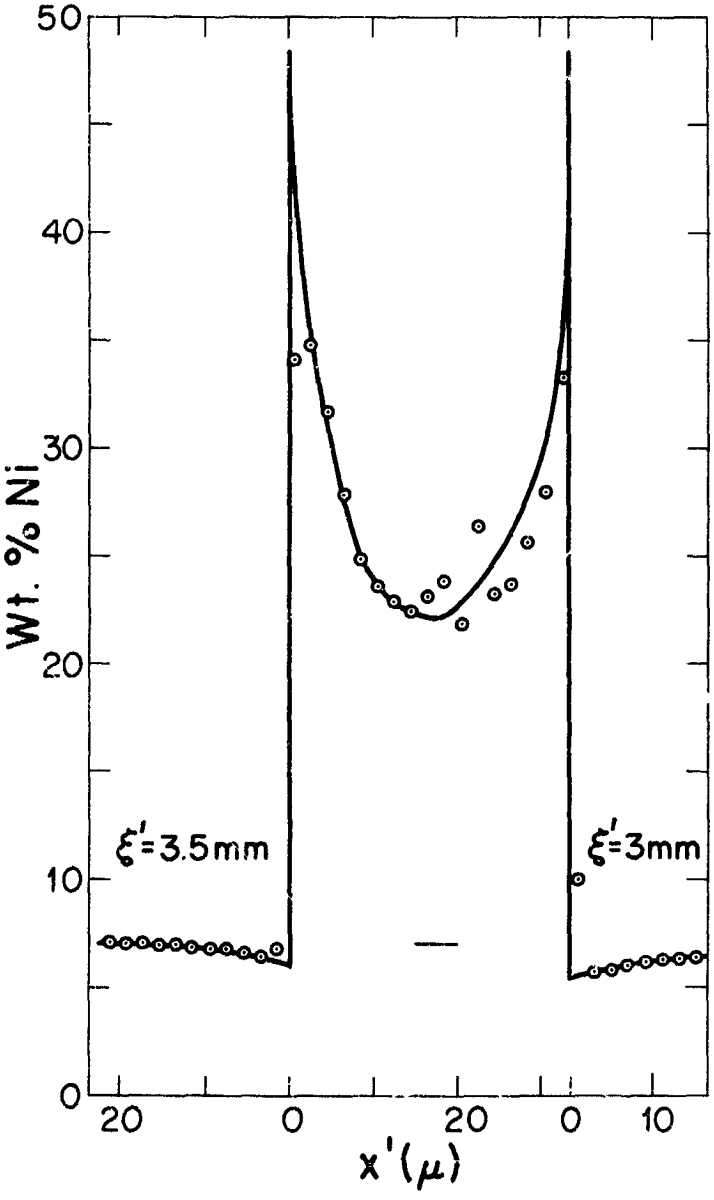

Figure 3

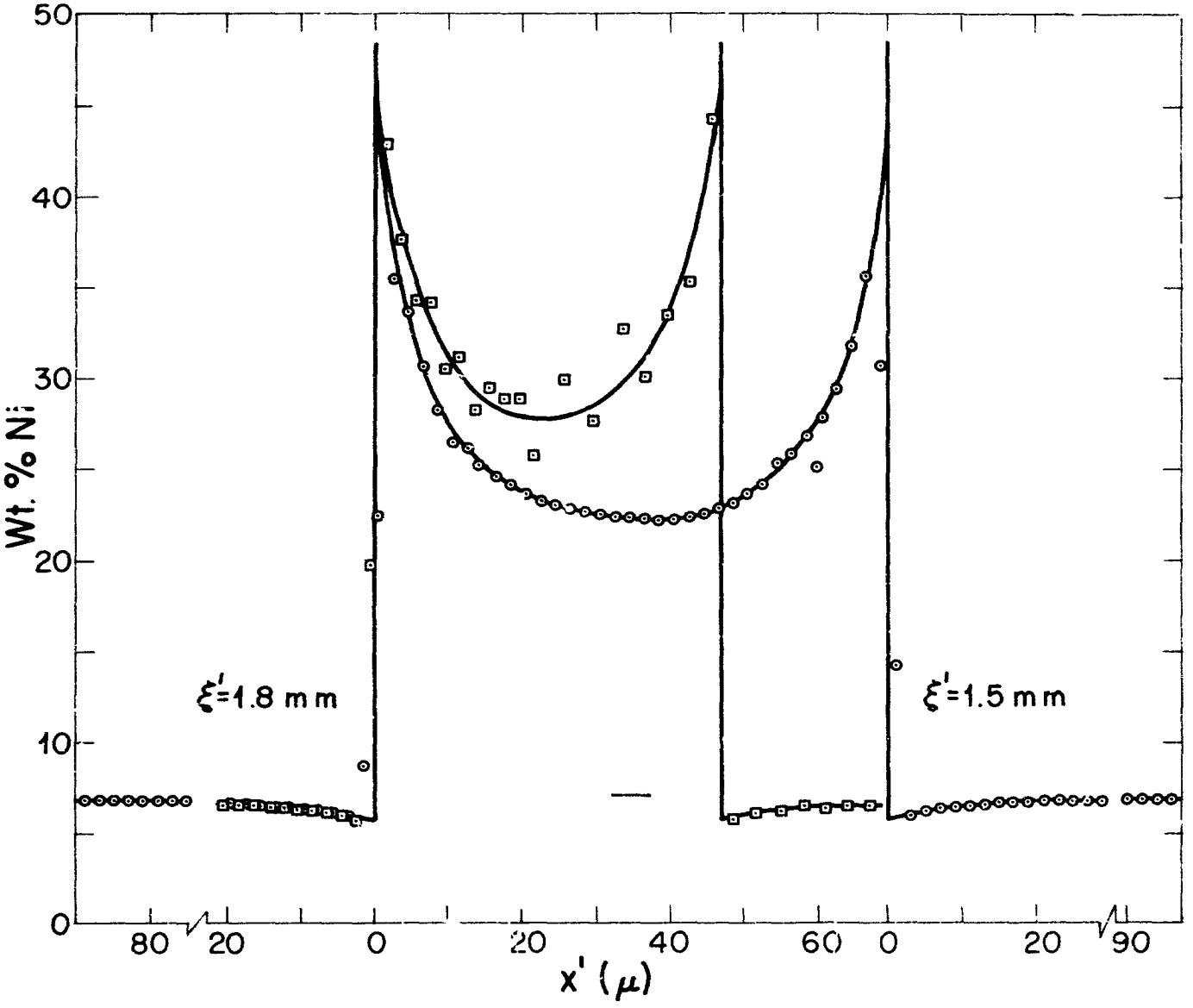

Figure 4

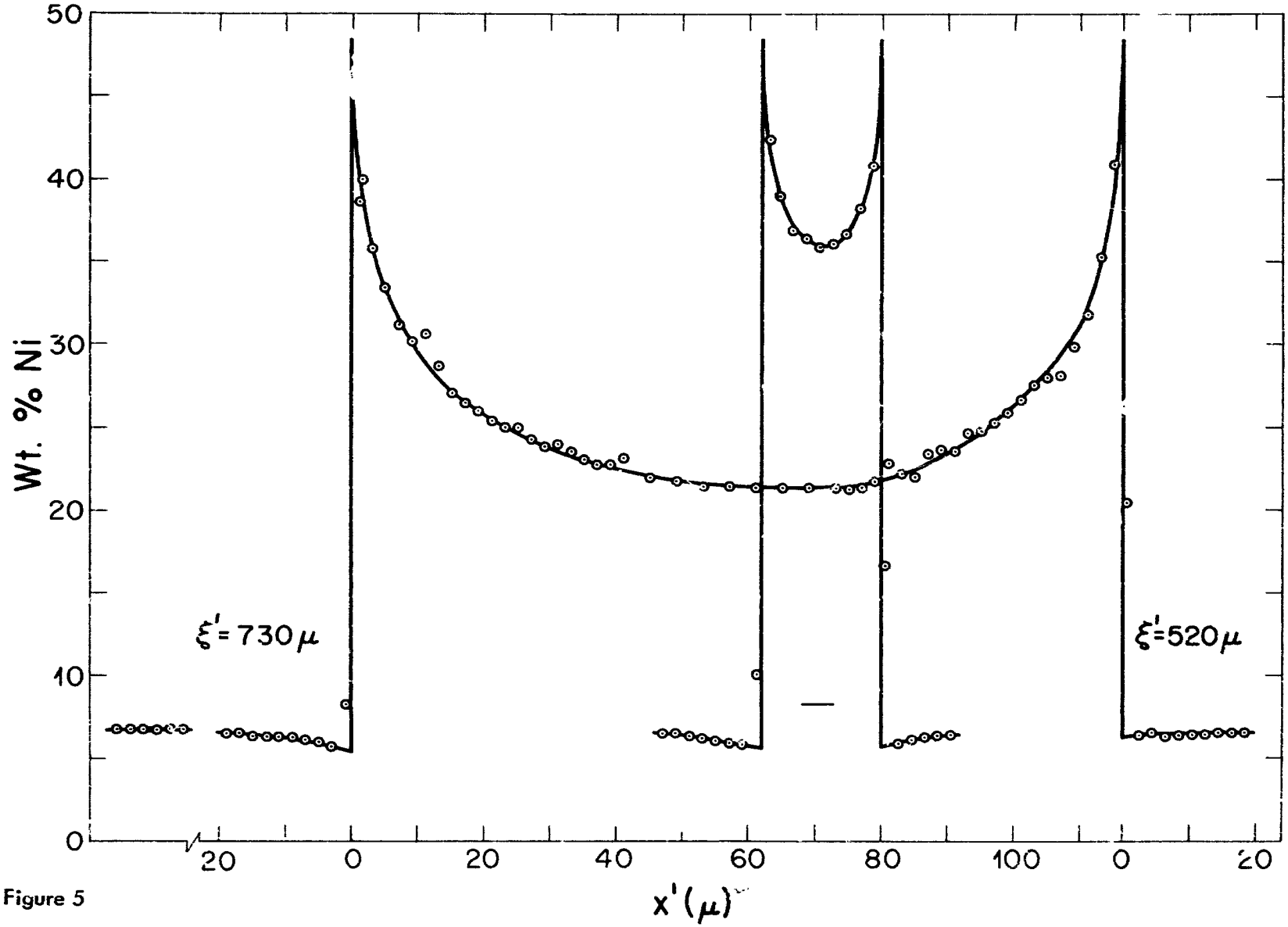

Figure 5

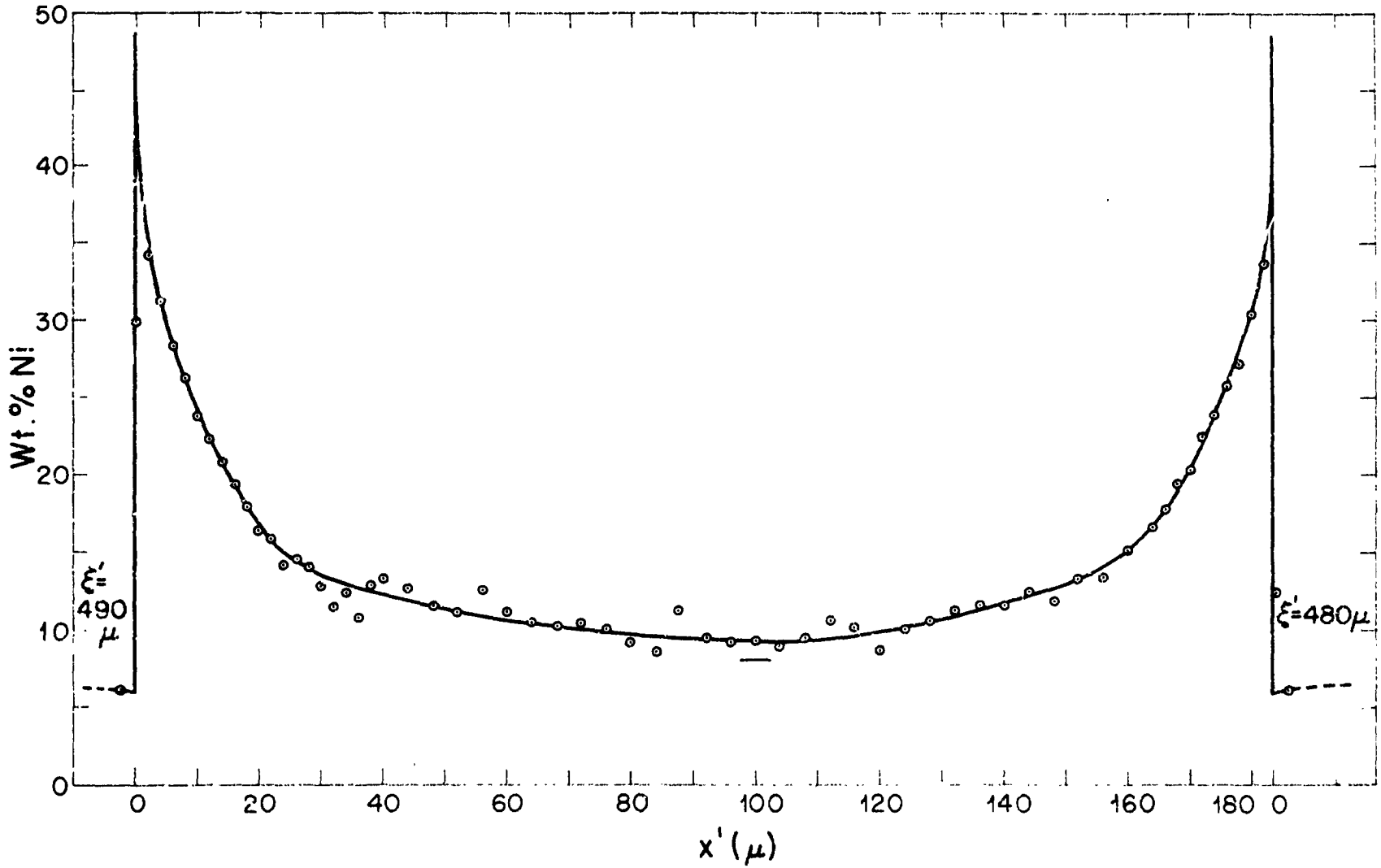
50
40
30
20
10
0
Wt. % Ni
ξ'= 490 μ
ξ'=480μ
0
20
40
60
80
100
120
140
160
180
0
x' (μ)

Figure 6

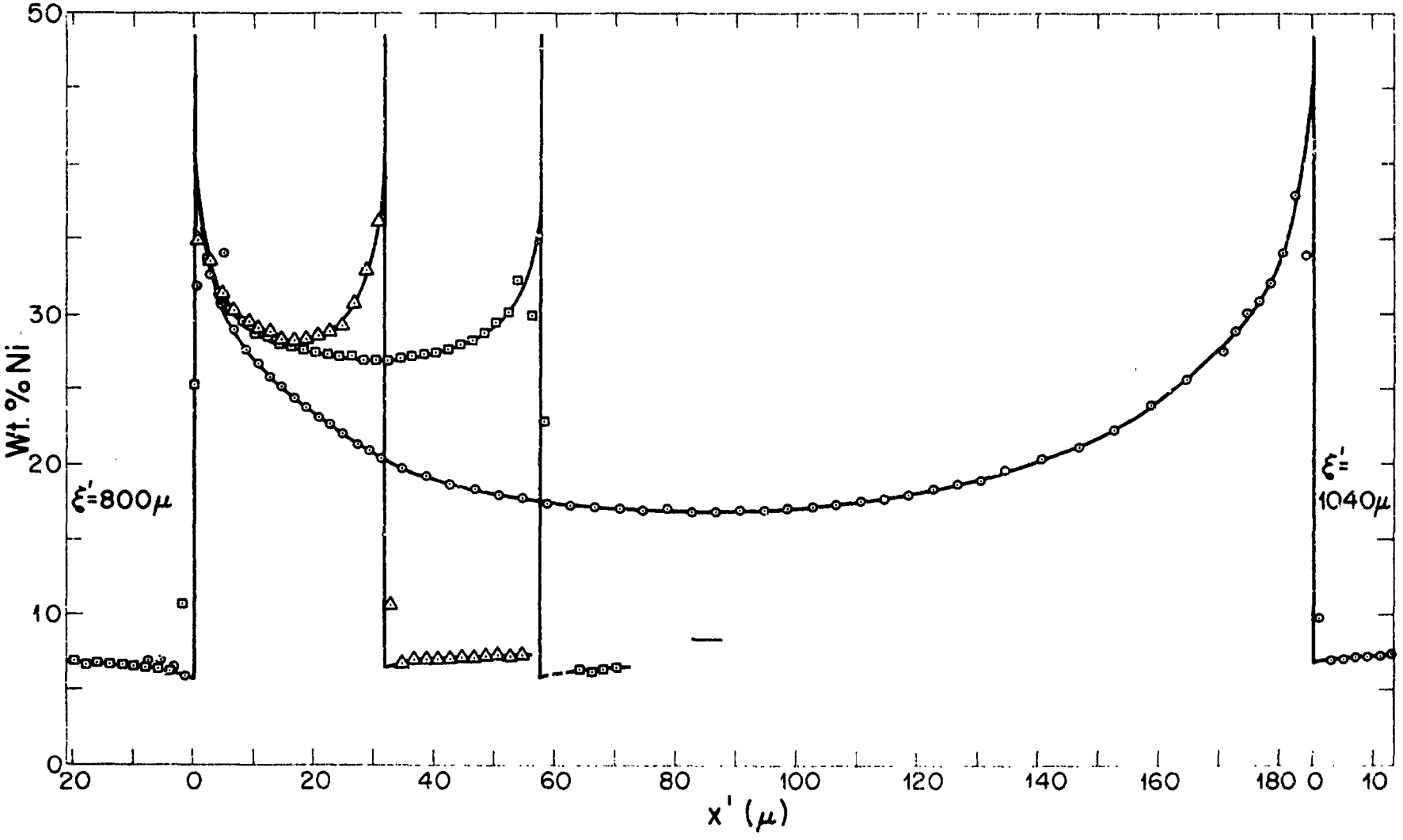
50
30
20
10
0
Wt. % Ni
ξ'=800μ
ξ'=
1040μ
20
0
20
40
60
80
100
120
140
160
180
0
10
x' (μ)

Figure 7

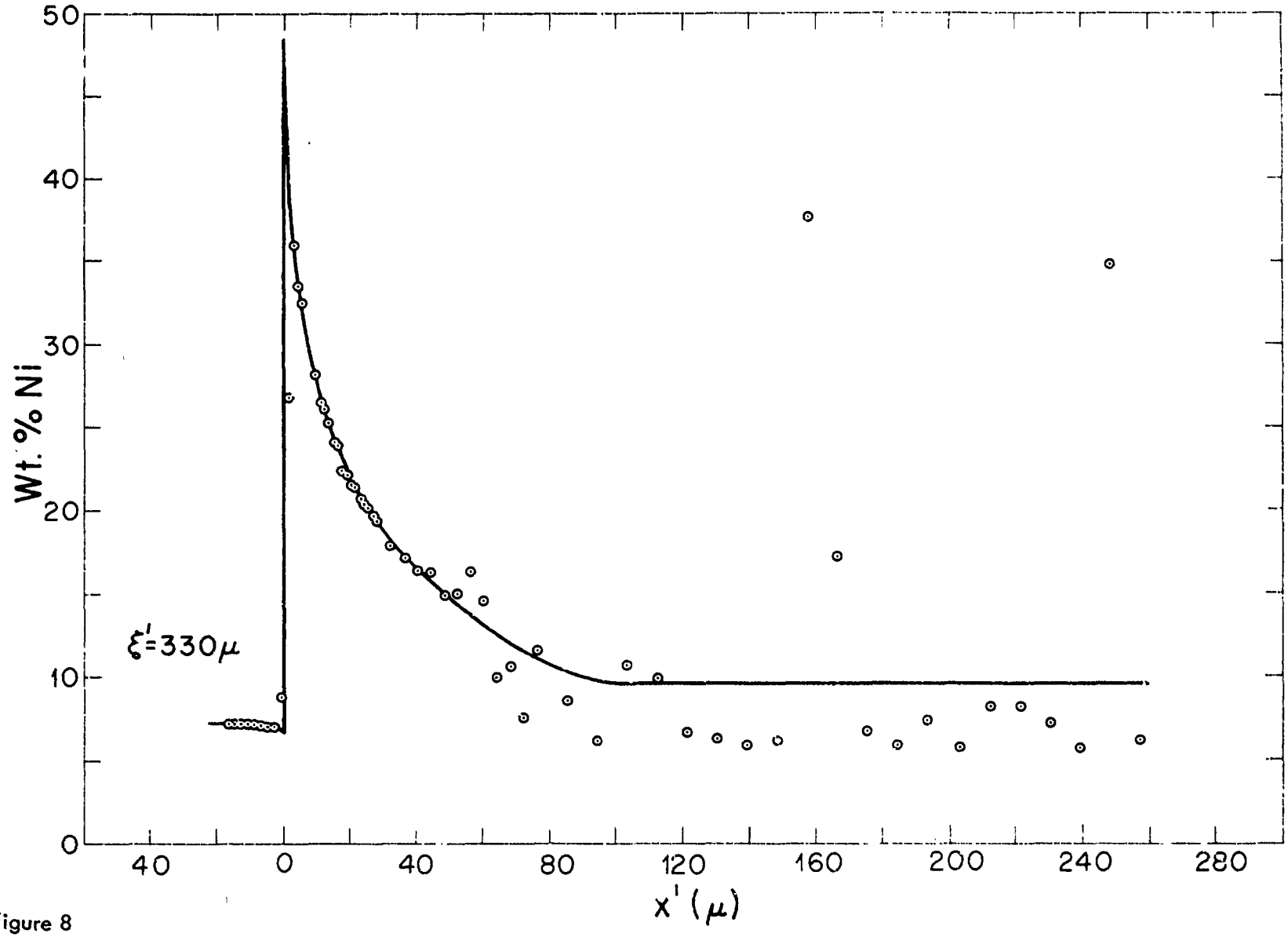

Figure 8

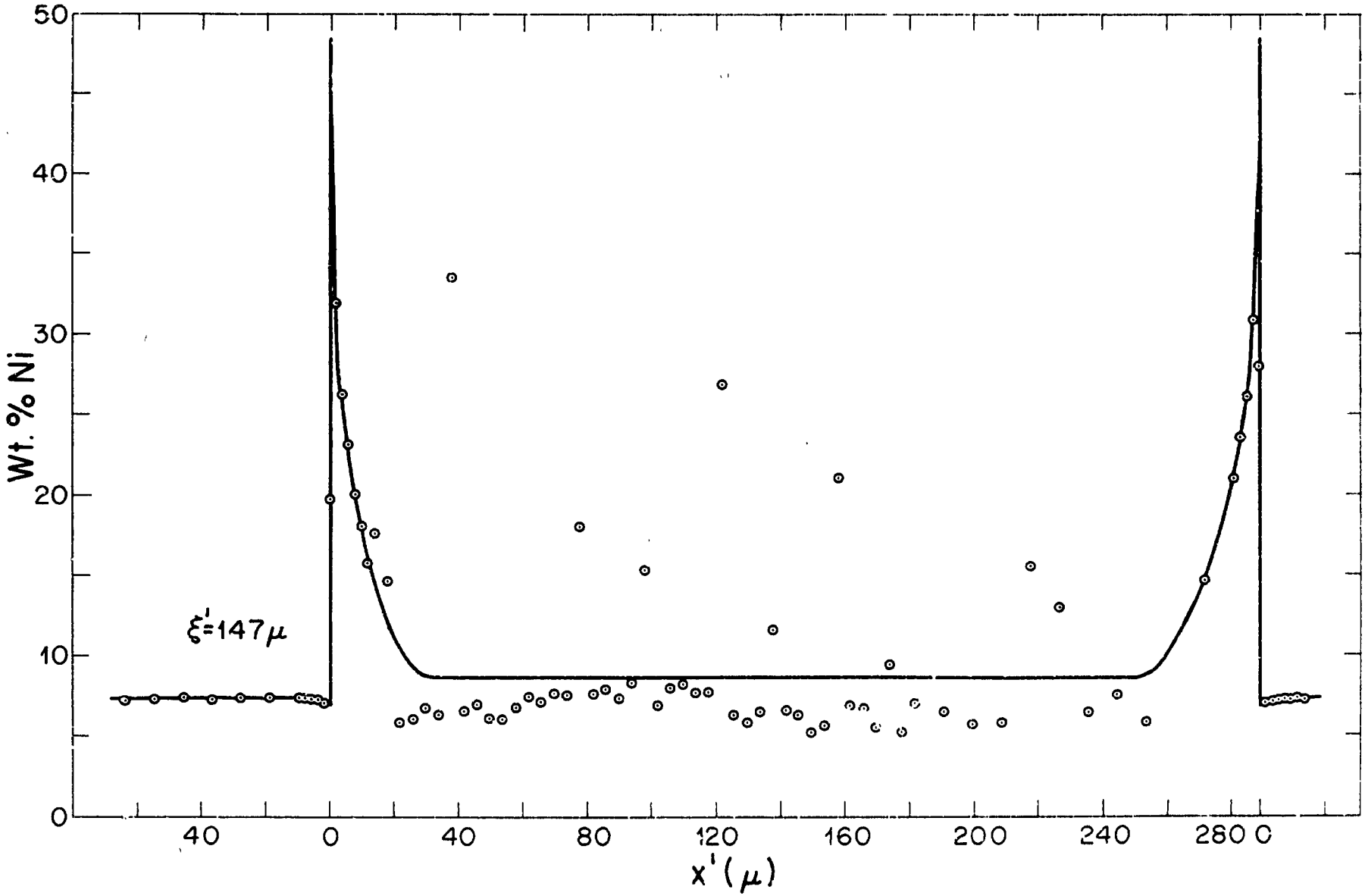

Figure 9

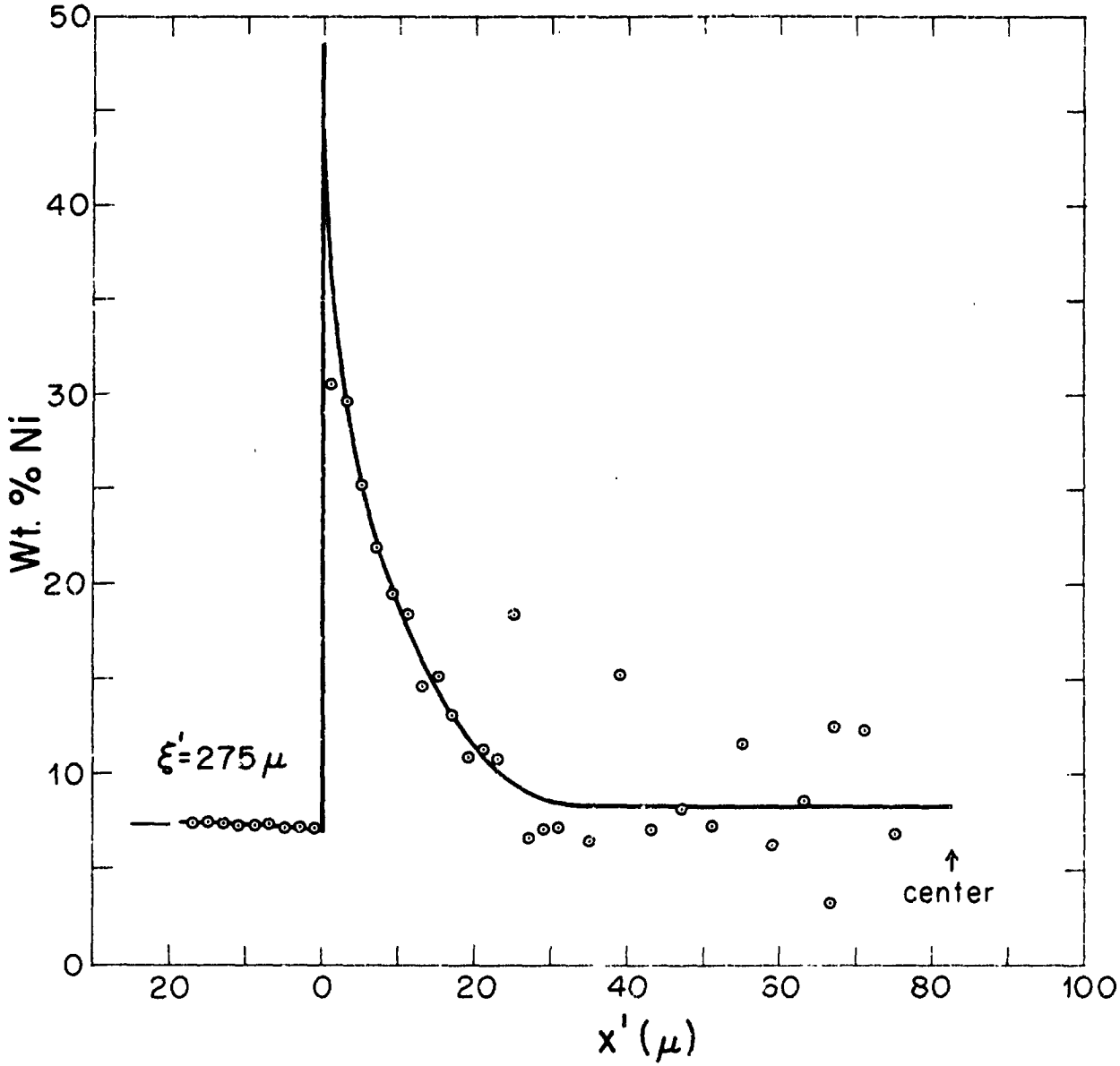

Figure 10

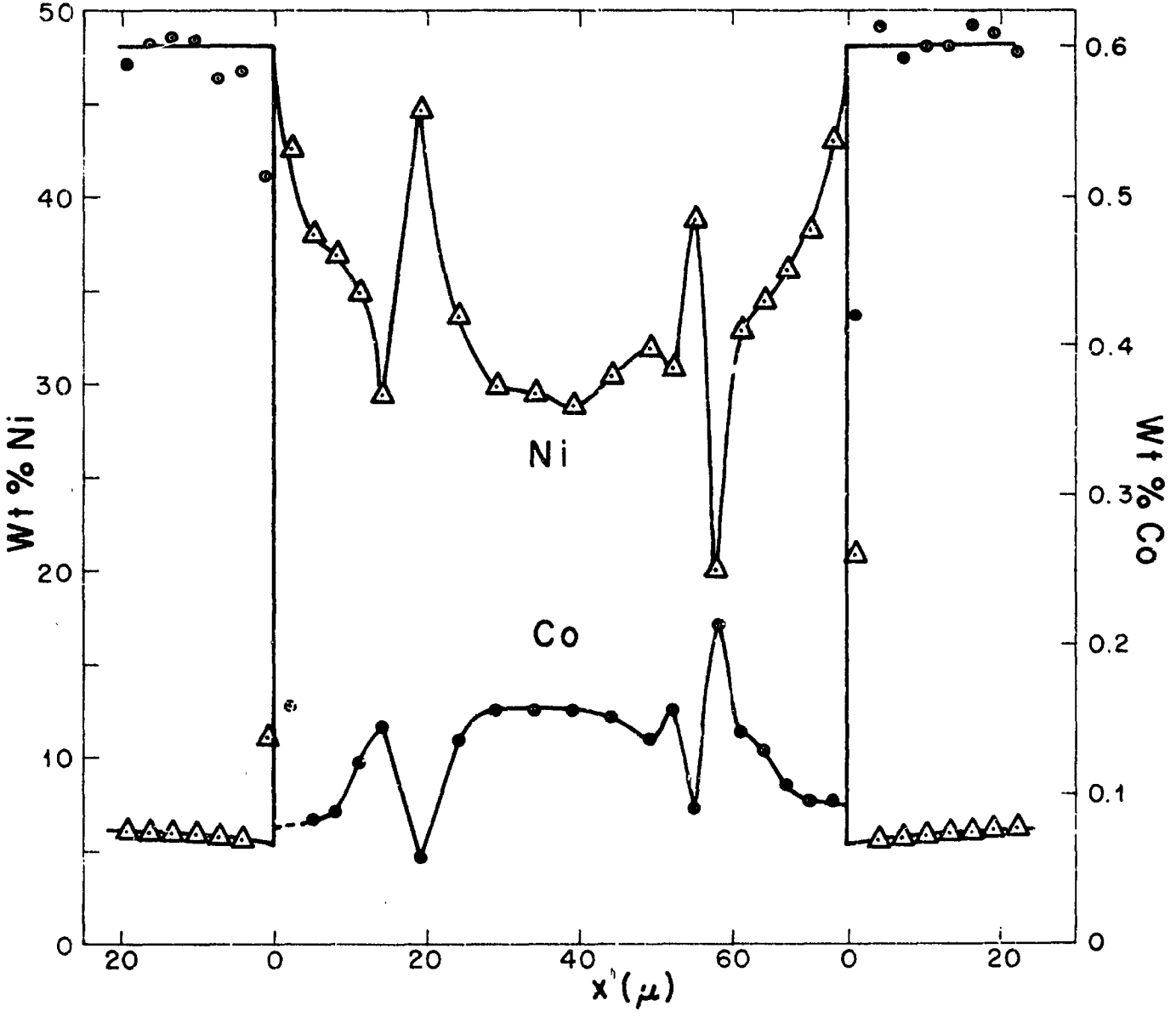
50
40
30
20
10
0
Wt % Ni
0.6
0.5
0.4
0.3
0.2
0.1
0
Wt % Co
Ni
Co
20
0
20
40
60
0
20
x' (μ)

Figure II

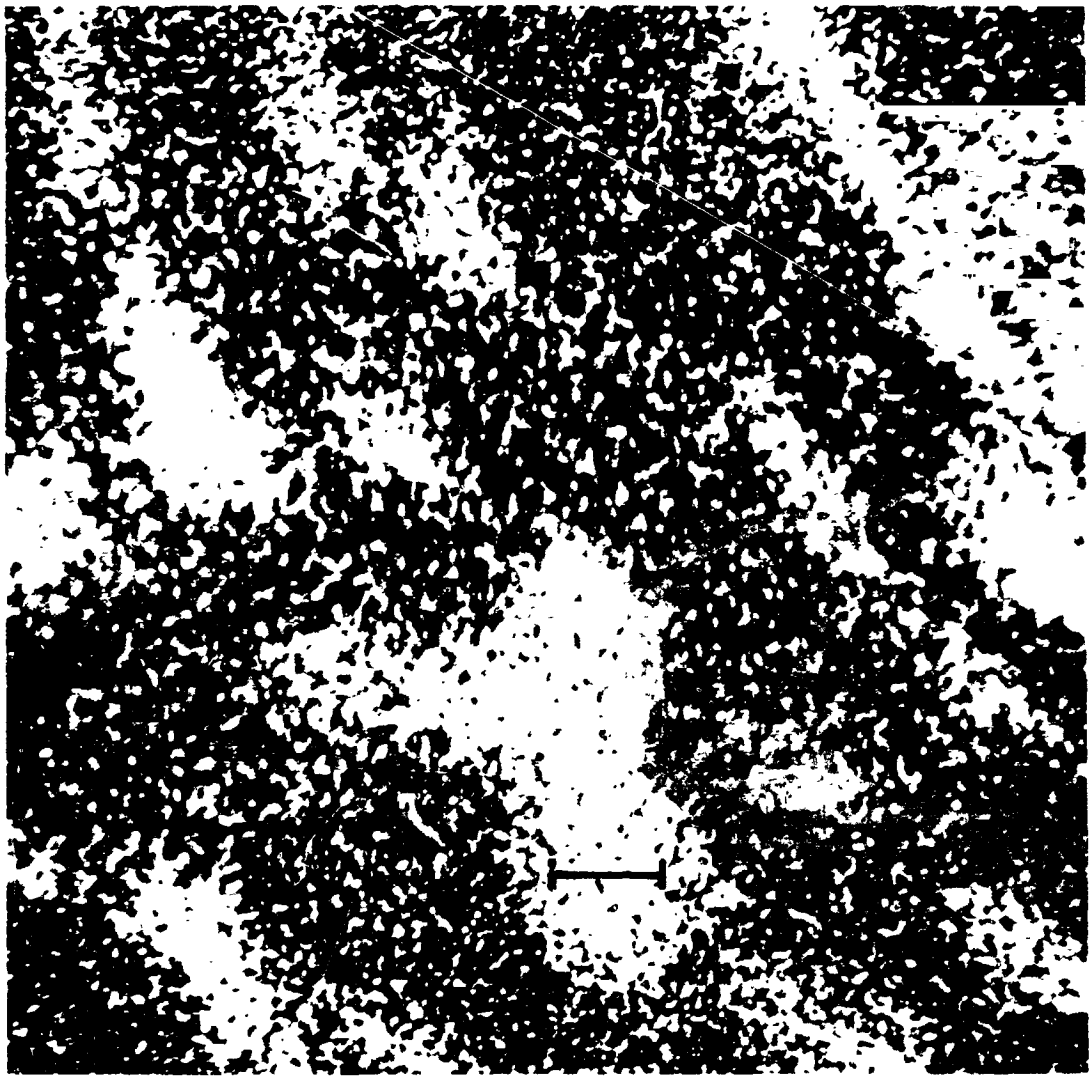

Figure 12

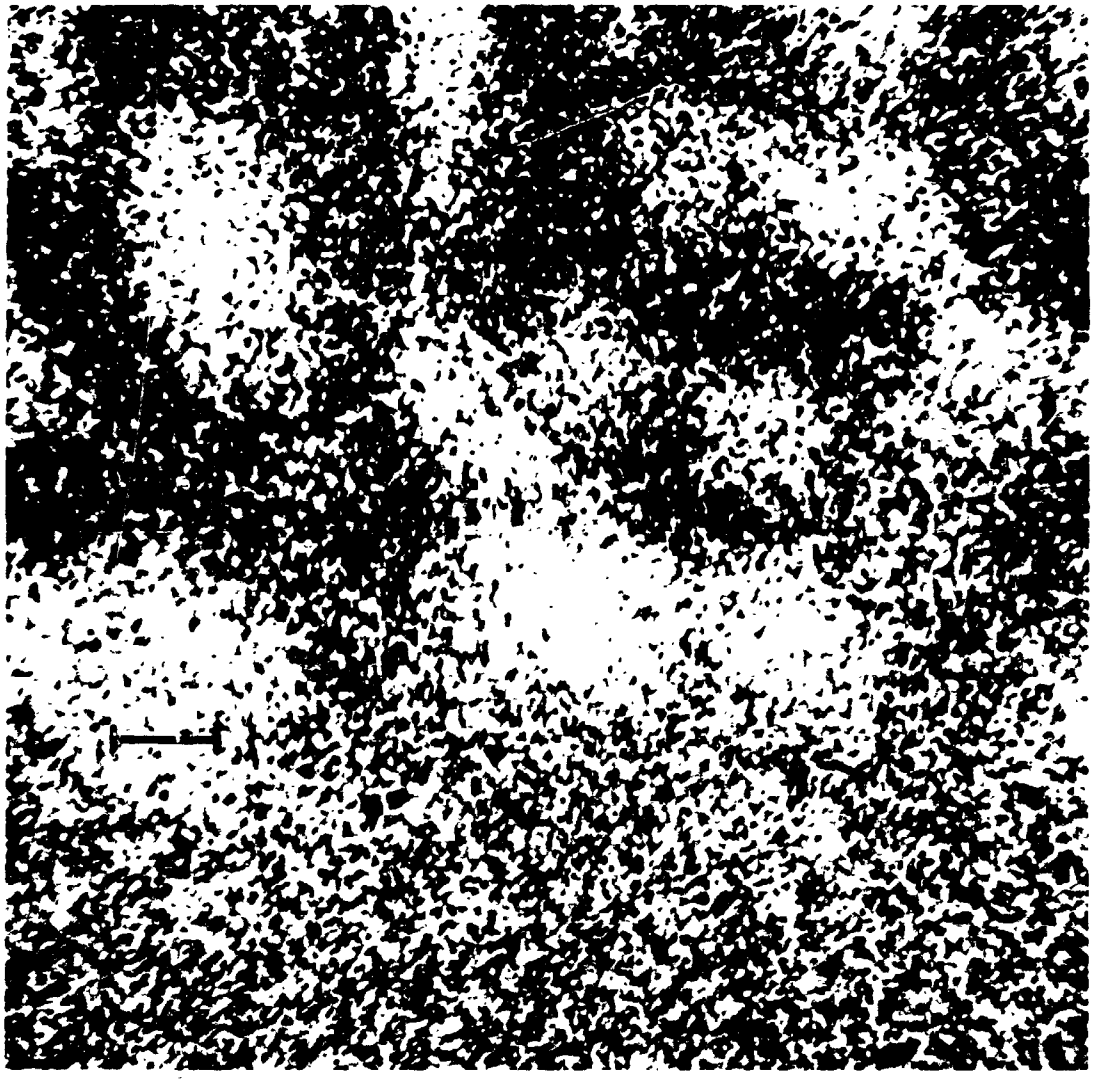

Figure 13

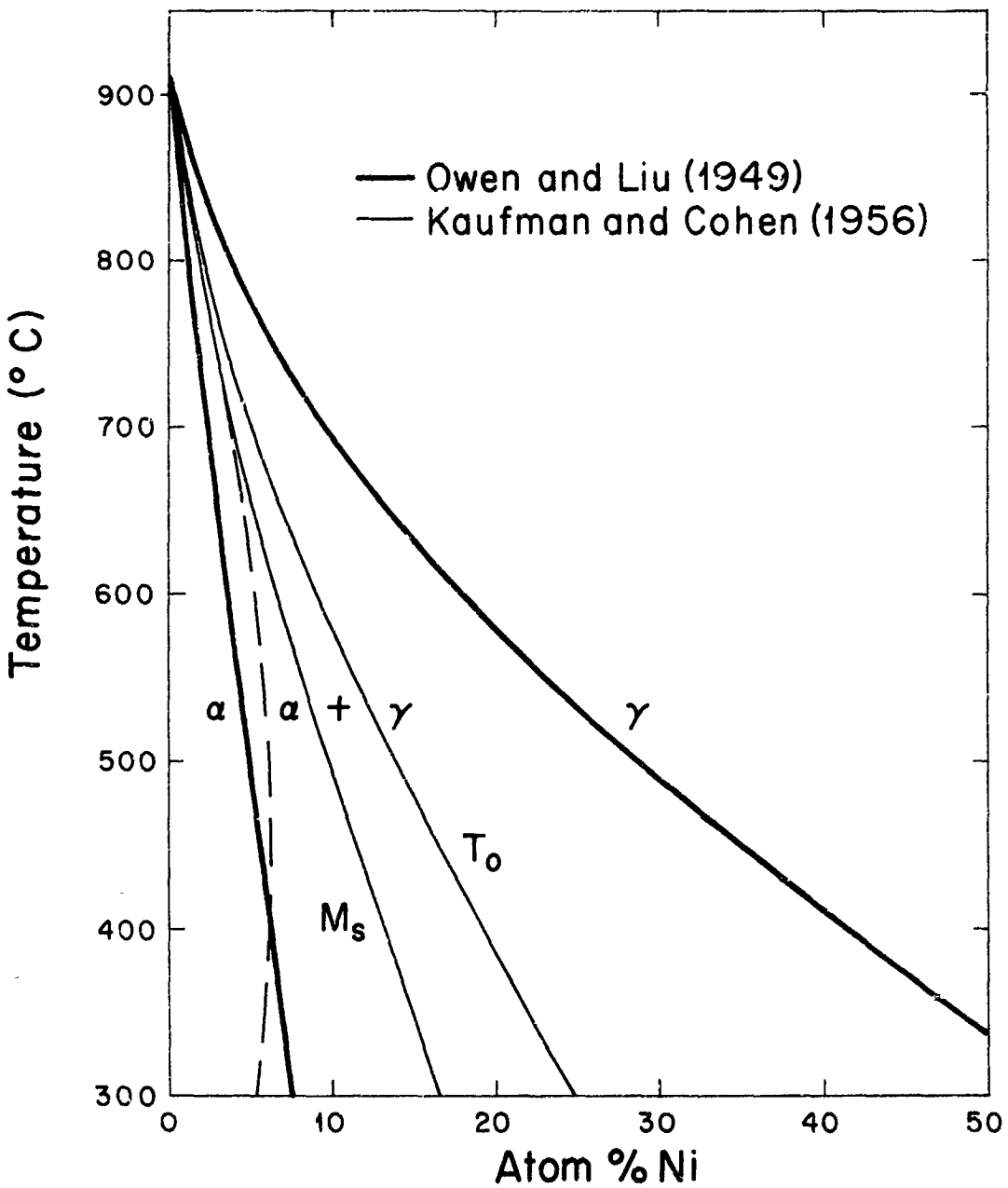
Owen and Liu (1949)
Kaufman and Cohen (1956)
Temperature (° C)
900
800
700
600
500
400
300
0
10
20
30
40
50
Atom % Ni
α
α + γ
γ
γ
T_o
M_s

Figure 14

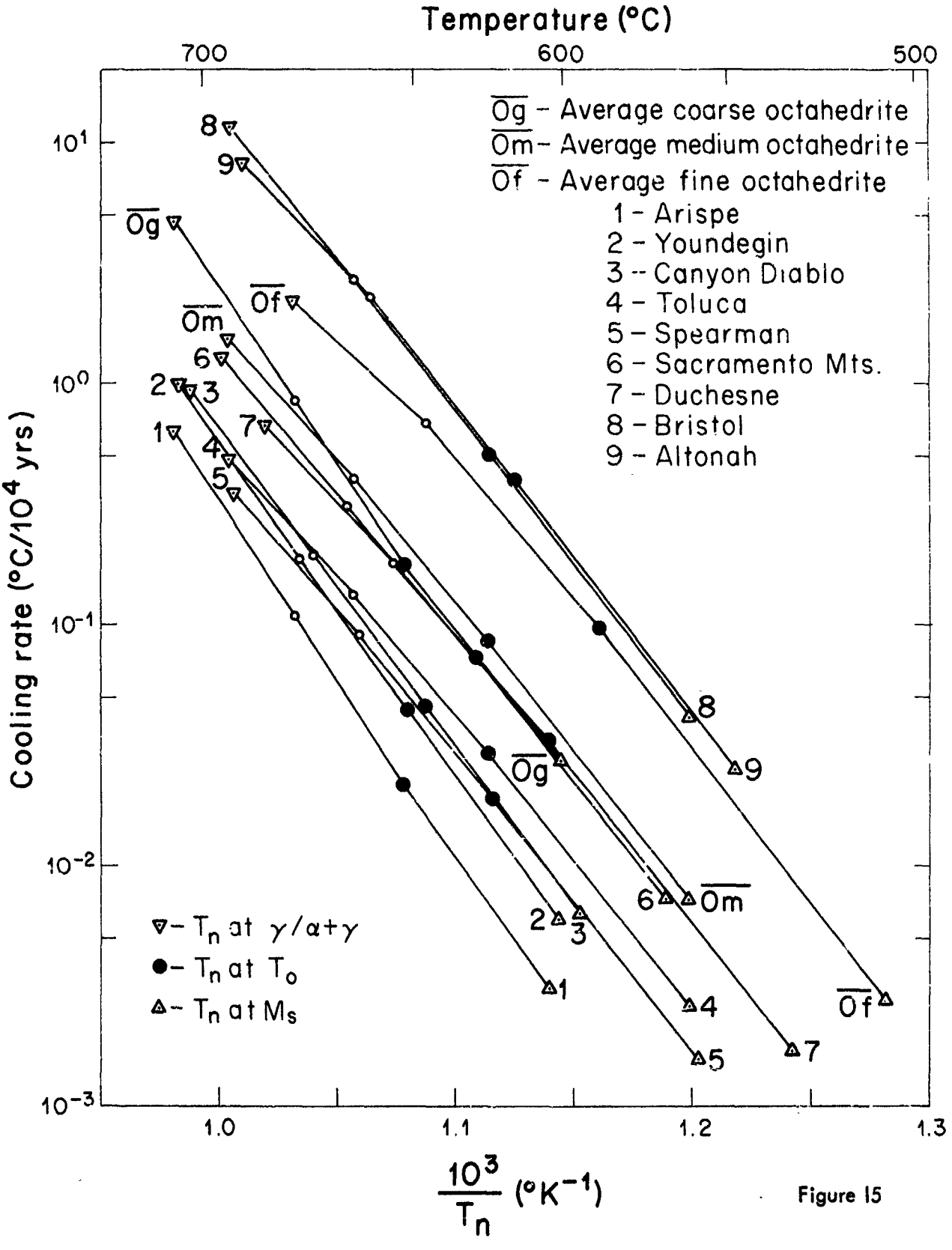
Temperature (°C)
700
600
500
Og – Average coarse octahedrite
Om – Average medium octahedrite
Of – Average fine octahedrite
1 – Arispe
2 – Youndegin
3 – Canyon Diablo
4 – Toluca
5 – Spearman
6 – Sacramento Mts.
7 – Duchesne
8 – Bristol
9 – Altonah
Cooling rate (°C/10⁴ yrs)
10¹
10⁰
10⁻¹
10⁻²
10⁻³
▽ – Tn at γ/α+γ
● – Tn at To
△ – Tn at Ms
1.0
1.1
1.2
1.3
10³/Tn (°K⁻¹)

Figure 15

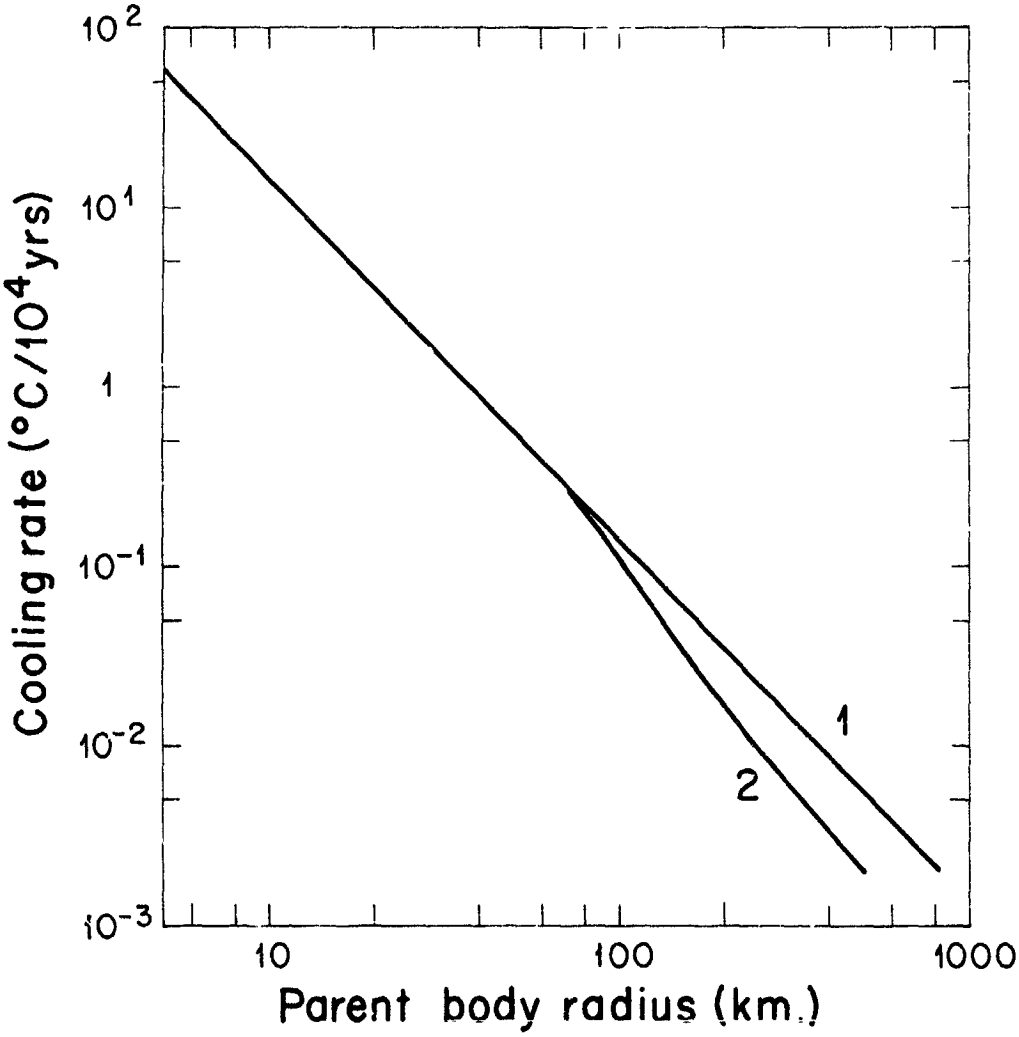
10^2
10^1
1
10^{-1}
10^{-2}
10^{-3}
Cooling rate (°C/10^4yrs)
10
100
1000
Parent body radius (km.)
1
2

Figure 16

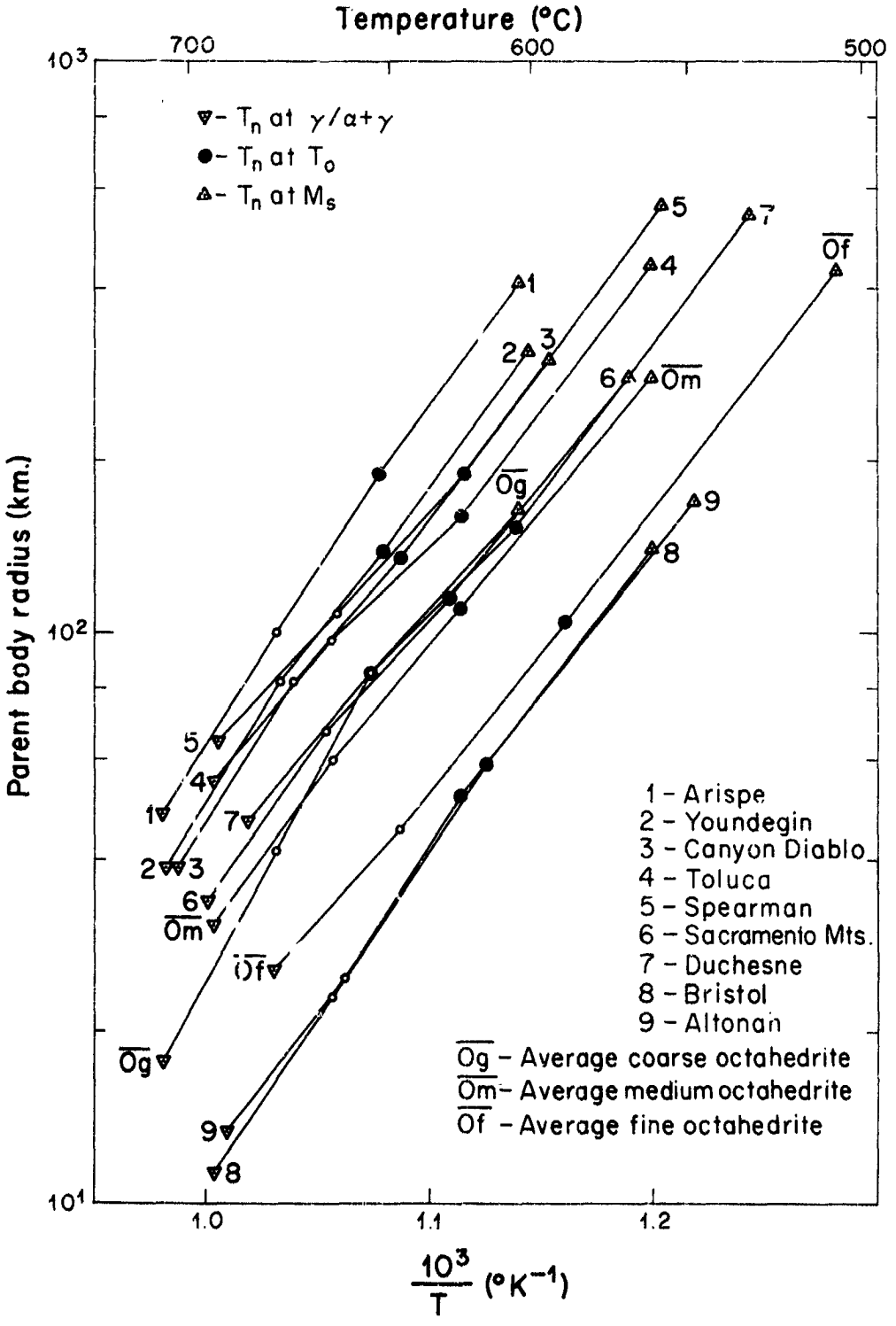
Temperature (°C)
700
600
500
10^3
10^2
10^1
▽- T_n at $\gamma/\alpha+\gamma$
●- T_n at T_o
△- T_n at M_s
Parent body radius (km.)
1 - Arispe
2 - Youndegin
3 - Canyon Diablo
4 - Toluca
5 - Spearman
6 - Sacramento Mts.
7 - Duchesne
8 - Bristol
9 - Altonan
$\overline{Og}$ - Average coarse octahedrite
$\overline{Om}$ - Average medium octahedrite
$\overline{Of}$ - Average fine octahedrite
1.0
1.1
1.2
$\frac{10^3}{T}$ (°K^{-1})

Figure 17

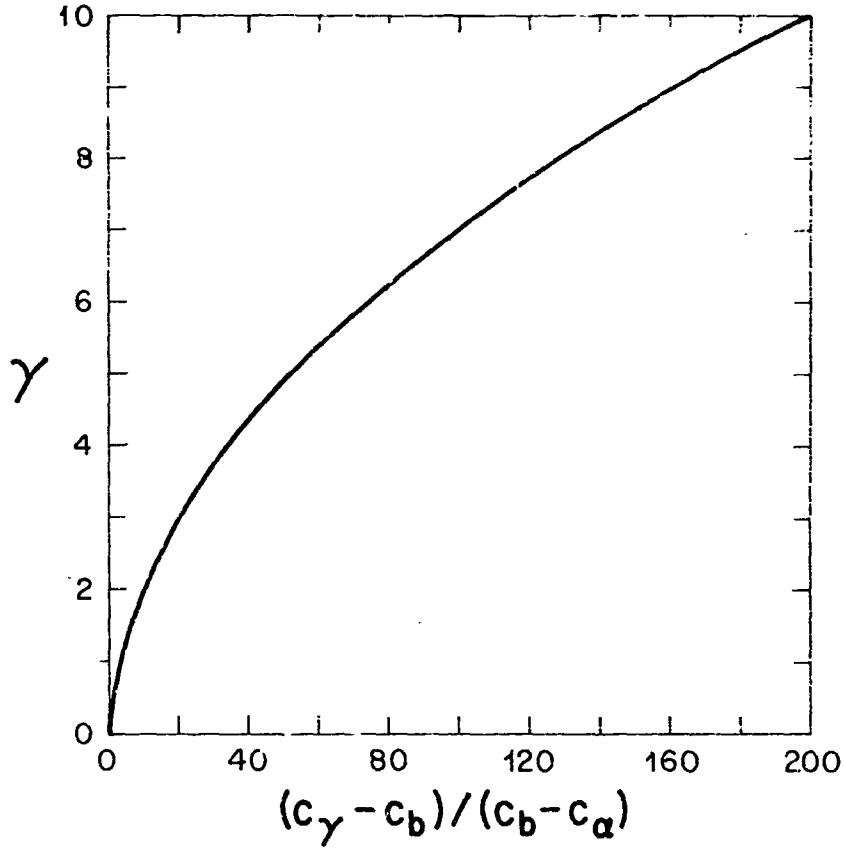

Figure 18